frontiers | Frontiers in Chemistry

TYPE Review
PUBLISHED 10 March 2023
DOI 10.3389/fchem.2023.1162183

OPEN ACCESS

EDITED BY
Guigao Liu,
Nanjing University of Science and Technology, China

REVIEWED BY
Xiubing Huang,
University of Science and Technology Beijing, China
Nan Zhang,
Hunan University, China

*CORRESPONDENCE
Huimin Liu,
liuhuimin08@tsinghua.org.cn

SPECIALTY SECTION
This article was submitted to Catalytic Reactions and Chemistry, a section of the journal Frontiers in Chemistry

RECEIVED 09 February 2023
ACCEPTED 27 February 2023
PUBLISHED 10 March 2023

CITATION
Guo J, Liu H, Li Y, Li D and He D (2023), Recent advances on catalysts for photocatalytic selective hydrogenation of nitrobenzene to aniline.
Front. Chem. 11:1162183.
doi: 10.3389/fchem.2023.1162183

Recent advances on catalysts for photocatalytic selective hydrogenation of nitrobenzene to aniline

Jiawen Guo[1], Huimin Liu[1]*, Yuqiao Li[1], Dezheng Li[1] and Dehua He[2]

[1]School of Chemical and Environmental Engineering, Liaoning University of Technology, Jinzhou, China, [2]Innovative Catalysis Program, Key Lab of Organic Optoelectronics and Molecular Engineering of Ministry of Education, Department of Chemistry, Tsinghua University, Beijing, China

Selective hydrogenation of nitrobenzene (SHN) is an important approach to synthesize aniline, an essential intermediate with extremely high research significance and value in the fields of textiles, pharmaceuticals and dyes. SHN reaction requires high temperature and high hydrogen pressure *via* the conventional thermal-driven catalytic process. On the contrary, photocatalysis provides an avenue to achieve high nitrobenzene conversion and high selectivity towards aniline at room temperature and low hydrogen pressure, which is in line with the sustainable development strategies. Designing efficient photocatalysts is a crucial step in SHN. Up to now, several photocatalysts have been explored for photocatalytic SHN, such as TiO_2, CdS, Cu/graphene and Eosin Y. In this review, we divide the photocatalysts into three categories based on the characteristics of the light harvesting units, including semiconductors, plasmonic metal-based catalysts and dyes. The recent progress of the three categories of photocatalysts is summarized, the challenges and opportunities are pointed out and the future development prospects are described. It aims to give a clear picture to the catalysis community and stimulate more efforts in this research area.

KEYWORDS

photocatalysis, selective hydrogenation of nitrobenzene, semiconductor, plasmonic metal-based catalyst, dye

1 Introduction

Aniline is one of the important amine substances and an essential intermediate for the synthesis of organic chemical raw materials. It is mainly used for the production of textiles, medicine, rubber auxiliaries, dyes and others, and has extremely high research significance and value (Junhua et al., 2010; Maji et al., 2011; Jiang et al., 2015; Wang et al., 2015; Kou et al., 2017). Aniline could be synthesized *via* the following approaches, such as chlorophenyl amination (Chen et al., 2009), direct ammonization (Wang et al., 2019a) and selective hydrogenation of nitrobenzene (SHN) (Wei et al., 2014). Notably, the selectivity towards aniline in SHN is high since few side reactions accompany the SHN main reaction, which makes it as the most simple, clean and efficient approach for the synthesis of aniline.

In a conventional thermal-driven catalytic process, SHN requires high temperature and high hydrogen pressure to achieve high yields of aniline. On the contrary, photocatalysis can realize high nitrobenzene conversion and high selectivity to aniline at room temperature and

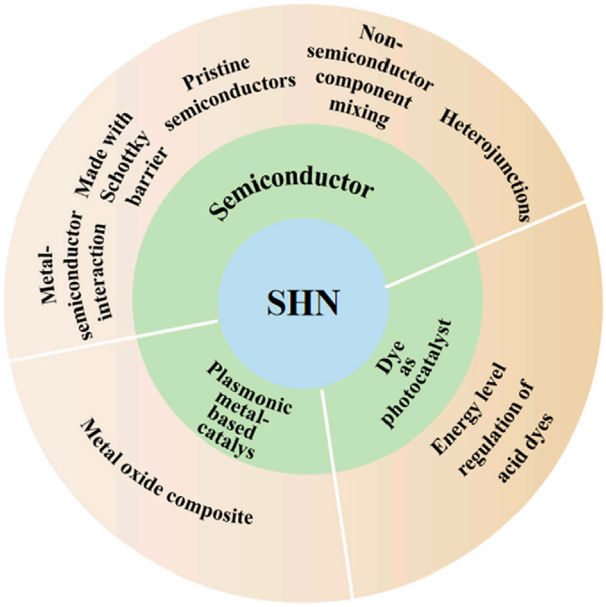

SCHEME 1
Strategies for photocatalytic selective hydrogenation of nitrobenzene to aniline.

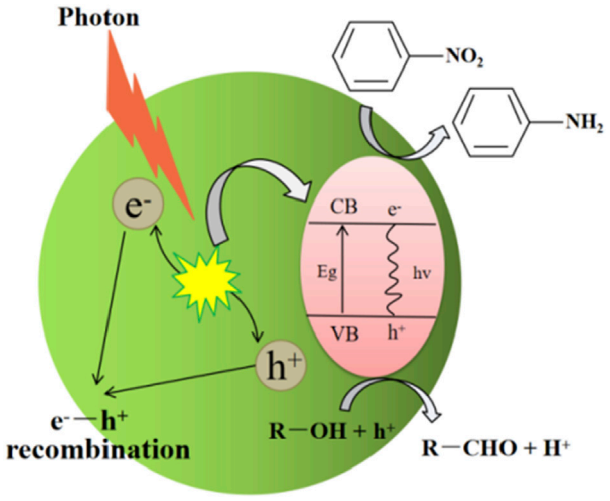

SCHEME 2
Mechanism of SHN catalyzed by a semiconductor, where alcohol (R-OH) is used as a hole scavenger.

low hydrogen pressure (Tsutsumi et al., 2016; Jiang et al., 2021), which reduces energy consumption and is in line with the sustainable development strategies.

In most chemical reactions, catalysts play important roles in reducing the activation energies and increasing the reaction rates. Researchers are committed to developing an efficient SHN photocatalyst. Up to now, several photocatalysts for photocatalytic SHN reaction have been developed, including TiO_2, CdS, Cu/graphene, and Eosin Y. In this review, we divide the photocatalysts into three categories based on the nature of the light harvesting units, which are semiconductors, plasmonic metal-based catalysts and dyes (Scheme 1), respectively. The progress of photocatalysts for SHN are reviewed and mechanisms of various catalysts are illustrated, aiming at providing a methodical summary and inspiring more researches to develop the fields of photocatalysis and nitrobenzene hydrogenation reaction.

2 Semiconductor

Since the discovery of photocatalysis by Fujishima et al. in 1972, the field of semiconductor photocatalysis has been opened up, the applications of semiconductors in a wide variety of reactions have been extensively studied, and the mechanism of semiconductors in photocatalytic reactions have been generalized (Akhundi et al., 2022; Murali et al., 2022; Fujishima et al., 2000).

The energy band structure of a semiconductor is usually composed of a low-energy valence band (VB) filled with electrons and an empty high-energy conduction band (CB). When light is irradiated onto a semiconductor, if the energy of the photon is greater than or equal to the semiconductor band gap (BG), the electrons in VB of the semiconductor will be excited to CB, and meanwhile, holes are generated in VB (Fujishima et al., 2000; Xuan and Xiao, 2012; Wang et al., 2019b).

Electrons and holes generated by photoexcitation migrate to the surface of the semiconductor for redox reactions. The photogenerated holes in VB have a strong oxidizing ability, which can capture the adsorbed substances on the surface of the semiconductor or electrons in the solvent (served as scavengers) and oxidize low-valent ions into high-valent ions. The electrons transitioning to CB are of strong reducing ability, which can be received by the electron acceptor on the semiconductor surface or holes in the solvent (served as scavengers) and reduce high-valent ions to low-valent ions (Fukui et al., 2019; Roy, 2020; Yun et al., 2020). For SHN, the electrons undergo the reduction half reaction with nitrobenzene adsorbed on the surface while holes oxidize the adsorbed hydrogen species or hole scavengers.

In terms of thermodynamics, the photocatalytic reaction requires that the redox potential of the electron donor is lower than the redox potential of the VB, while the redox potential of the electron acceptor should be higher than the redox potential of the CB (Buzzetti et al., 2019). Theoretically, when the CB position of a semiconductor is lower than −0.486 V, nitrobenzene can be photocatalytically reduced to aniline ($E^{\theta}(C_6H_5NO_2/C_6H_5NH_2)$ = −0.486 V, vs. NHE). The oxidation reaction potential on electron acceptor depends on the type of reaction environment. If hydrogen is used as a reactant and directly oxidized at VB, the VB position of a semiconductor should be higher than 0 V ($E^{\theta}(H^+/H)$ = −0 V, vs. NHE) (Gao et al., 2020). In the case that alcohols or sodium sulfite are used as scavengers, the VB position of a semiconductor should be higher than their redox potentials. For example, when methanol is used as a hole scavenger and it is oxidized to formaldehyde ($E^{\theta}(CH_3OH/CH_2O)$ = +2.62 V, vs. NHE), VB position should be higher than +2.62 V (Shen et al., 2021). The reaction mechanism of SHN is shown in Scheme 2, where alcohol is used as a hole scavenger.

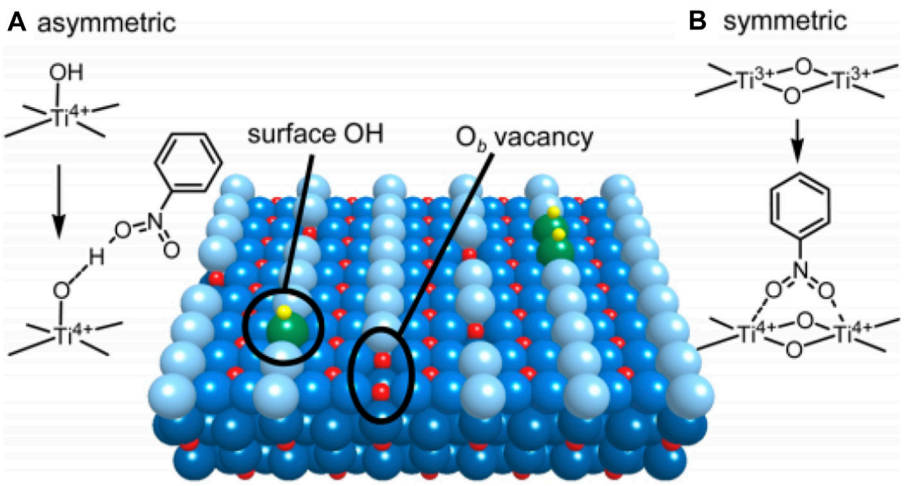

FIGURE 1
Surface structure of rutile TiO_2 (Yang et al., 2022). **(A)** Asymmetric adsorption mode of nitrobenzene, and **(B)** symmetric adsorption mode of nitrobenzene. Green and light blue spheres: O_b atom at [001] azimuth; yellow and red spheres: H and Ti atoms. Reproduced with permission from reference (Shiraishi et al., 2012).

Noteworthy, only the electrons and holes participated in redox reactions are beneficial for the photocatalytic performance. Some electrons and holes generated by photoexcitation may also recombine inside or on the surface of the semiconductor within a few milliseconds. Therefore, to improve the ability of the catalyst in the photoreduction of nitrobenzene, it is important to make full utilization of the photoexcited electron hole pairs and minimize the recombination of electrons and holes (Aljahdali et al., 2017; Abdullah et al., 2020).

Up to now, a series of semiconductors have been applied in photocatalytic SHN. In this section, we will describe the progress of photocatalytic SHN in each type of semiconductor photocatalysts as well as the modification approaches to improve their performance.

2.1 TiO_2

TiO_2 has been extensively studied in the field of photocatalysis due to its following advantages (Daghrir et al., 2013; Zhou et al., 2022): ① It is low-cost, safe and non-toxic; ② It has good light and chemical stability, and no photocorrosion or chemical corrosion will occur during the photocatalytic reactions; ③ It has a suitable BG, which allows it to be excited by ultraviolet light; ④ The photogenerated charges are of strong redox ability, which endows TiO_2 relatively high photocatalytic activity under ultraviolet irradiation (Tamaki et al., 2007; Qiu et al., 2014; Chaturvedi and Singh, 2021). These advantages of TiO_2 make it promising for photocatalytic SHN (Kandiel et al., 2014; Oliveira et al., 2016; Wang et al., 2016).

Shiraishi et al. (2012) research on the application of pristine TiO_2 in photocatalytic SHN is a typical example. The authors investigated the influence of crystalline structure of TiO_2 on the catalytic performance in SHN, where ethanol was used as the hydrogen source (Shiraishi et al., 2012). It suggested that commercial P25 and anatase TiO_2 were poor in SHN, resulting in unsatisfactory performance. On the contrary, rutile TiO_2 exhibited relatively high catalytic performance, with an almost complete nitrobenzene conversion and a selectivity towards aniline higher than 90.0%. Characterization results revealed that Ti atoms in the surface defects of rutile TiO_2 were the active sites. Rutile TiO_2 (Yang et al., 2022) surface was an alternating arrangement of coordinated 5-fold Ti^{4+} atoms and bridging O^{2-} atoms (O_b) running along the (001) direction (Figure 1) (Shiraishi et al., 2012). O_b vacancies were the surface defects, in which two excessive electrons related to O_b were transferred to the empty three-dimensional orbitals of adjacent Ti^{4+} atoms, resulting in two Ti^{3+} atoms. On the one hand, the adsorption sites of nitrobenzene were formed by surface Ti^{3+} atoms through electron transfer and served as capture sites for the light-formed CB e−. On the other hand, the Ti^{3+} atom on the surface of TiO_2 acted as the adsorption site of nitroaromatic hydrocarbons, and was the capture center of electron e− in the photoconduction band. Ti^{3+} atoms on the surface were both adsorption sites and electron capture centers. These two effects rapidly hydrogenated the nitrobenzene on the surface Ti^{3+} atoms to aniline and accelerated the reaction (Shiraishi et al., 2012).

Although rutile TiO_2 could catalyze photocatalytic SHN, it could only absorb ultraviolet light and the light utilization efficiency is low, which could not meet expectations. Therefore, further modification is necessary. At present, plenty of modification approaches have been developed and applied to the modification of pristine semiconductors, including fabricating a catalyst with Schottky barrier, constructing a heterojunction photocatalyst with another semiconductor and constructing a hybrid catalyst with non-semiconductor component.

① Fabricating a catalyst with Schottky barrier. Metals and semiconductors can form a Mott-Schottky junction, which is a simple metal-semiconductor interface, where electrons flow directionally between the metal and the semiconductor, with non-linear impedance characteristics (Lin et al., 2019; Kw et al.,

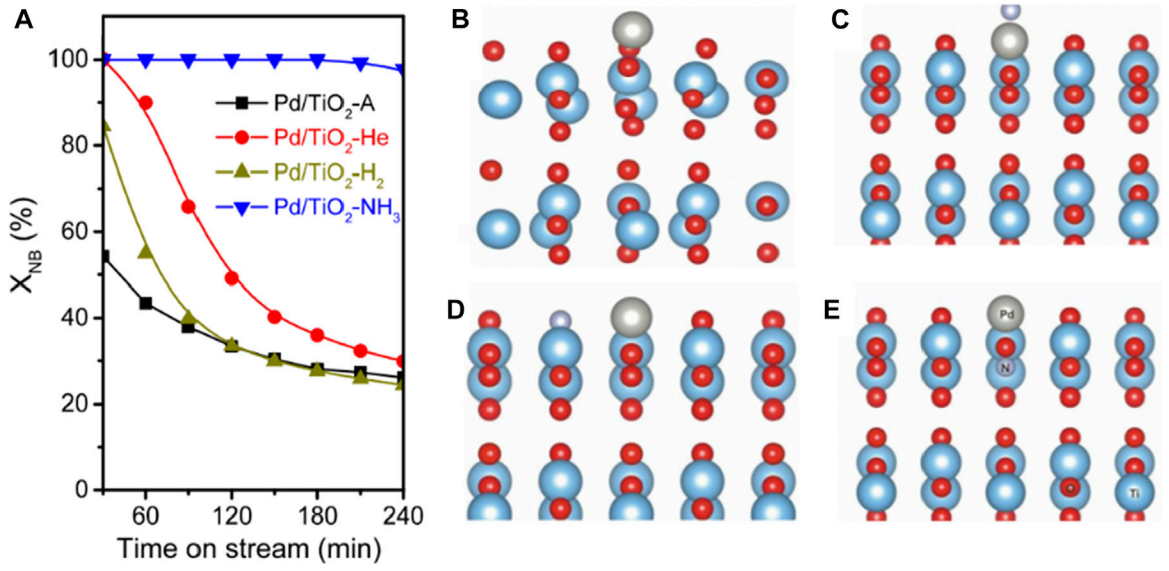

FIGURE 2
(A) Transitory conversion of nitrobenzene over Pd/TiO_2 catalyst at 160°C. A side view of the optimized structures for Pd/TiO_2 systems, with a Pd atom deposited on **(B)** non-doped TiO_2, **(C)** TiO_2 with $N\text{-}_{adsorption}$ on the surface, **(D)** TiO_2 with $N\text{-}s_{ubstitution}$ on the surface and **(E)** TiO_2 with $N\text{-}_{substitution}$ in the subsurface region. Spheres in red: O, light blue: Ti, gray: Pd, light purple: N, and light pink: H. Reproduced with permission from reference (Chen et al., 2017).

2020; Žerjav et al., 2021). Schottky proposed a metal-semiconductor contact barrier model under ideal conditions that ignores the interface state, so it is called the Schottky barrier (Xu et al., 2023). Catalysts with Schottky barrier are generally of strong capacity to improve the separation of electron hole pairs, thereby exhibiting superior catalytic performance. In addition, the deposition of metals (for instance Au, Ag, Pt, Pd, and Ru) could change the surface properties of semiconductors as well as the deposited metals, enlarge the light absorption range of the catalyst to the visible light region, and ultimately contribute to the catalytic performance. With the maturity of the Schottky contact theory, the research of catalysts based on the Schottky barrier principle has gradually increased. Some typical examples are illustrated below.

The interaction between metal and semiconductor could exert functions on catalytic performance. Chen et al. (2017) treated commercial TiO_2 in He, H_2, and NH_3, respectively, and then deposited Pd nanoparticles on the pristine and modified TiO_2 and obtained four catalysts (denoted as Pd/TiO_2-A, Pd/TiO_2-He, Pd/TiO_2-H_2 and Pd/TiO_2-NH_3, respectively) for photocatalytic SHN. Pd/TiO_2-NH_3 exhibited high catalytic activity (Figure 2A, Pd/TiO_2-NH_3 exhibited an initial nitrobenzene conversion of ~100.0%, much higher than the reference catalysts Pd/TiO_2-A and Pd/TiO_2-H_2), and good stability in photocatalytic SHN (Figure 2A, Pd/TiO_2-NH_3 remained stable for at least 240 min; on the contrary, Pd/TiO_2-A gradually deactivated after 30 min while Pd/TiO_2-He and Pd/TiO_2-H_2 rapidly deactivated after 240 min). It revealed that there was a strong interaction between Pd and the support, which tailored the electronic state of Pd/TiO_2 catalyst and promoted the activity. Density function theory (DFT) calculations suggested that Pd was positively charged while N was negatively charged (Figures 2B–E). When Pd and N atoms were electronically coupled at the surface, a large number of electrons accumulated around the N nucleus, resulting in Pd-N pairs. Additionally, the doping of N into TiO_2 had a structure-promoting effect, which favored the dispersion of Pd species on TiO_2, affording more active sites and expediting the reaction (Chen et al., 2017).

Schottky barrier could enhance the electron hole separation efficiency and contribute to the catalytic performance (Kamegawa et al., 2012; Qiu et al., 2016). For instance, Kamegawa et al. (2012) modified the surface of Pt-TiO_2 with colorless 2, 3-dihydroxynaphthalene (2, 3-DN), thereby designing a visible light sensitive photocatalyst for photocatalytic SHN. It is demonstrated that the Pt nanoparticles supported on the surface of TiO_2 fully separated photogenerated electrons and holes, which endowed the catalyst 2,3-DN/Pt-TiO_2 high selectivity in photocatalytic SHN. Notably, 2,3-DN(1)/Pt-TiO_2 (where one describes the content of 2,3-DN) recorded an aniline yield of 75.0%, much higher than other catalysts (such as Pt-TiO_2 modified by hydroxynaphthalene and 2,3-DN/Pt-TiO_2 with other 2,3-DN contents). Qiu et al. (2016) designed a ternary-structured Pt-TiO_2-RGO (RGO: reduced graphene oxide) through sol-gel and microwave-assisted strategies, in which TiO_2 nanoparticles were grown *in situ* on GO sheets (Figure 3A) and Pt nanoparticles were stabilized on the surface of the TiO_2-RGO composites (Figure 3B). Over Pt-TiO_2-RGO catalyst, TiO_2 existed in the single crystal form (Figure 3C). RGO guaranteed good electrical conductivity of the catalyst, in which RGO not only acted as a stabilizer for TiO_2 nanocrystals and Pt nanoparticles but also served as a "power wire" that prevented electron and hole recombination. Under sunlight irradiation, the recombination

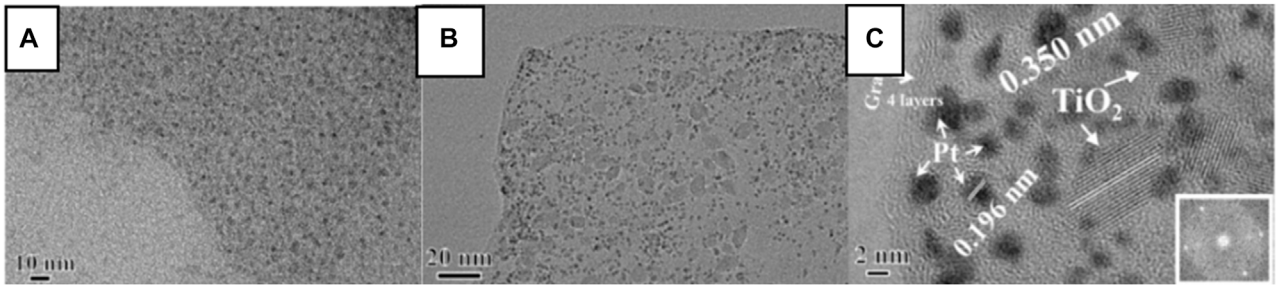

FIGURE 3
(A) High resolution transmission electron microscope (HRTEM) images of TiO_2-RGO, and **(B)** TEM and **(C)** HRTEM images of the Pt-TiO_2-RGO catalyst. Reproduced with permission from reference (Qiu et al., 2016).

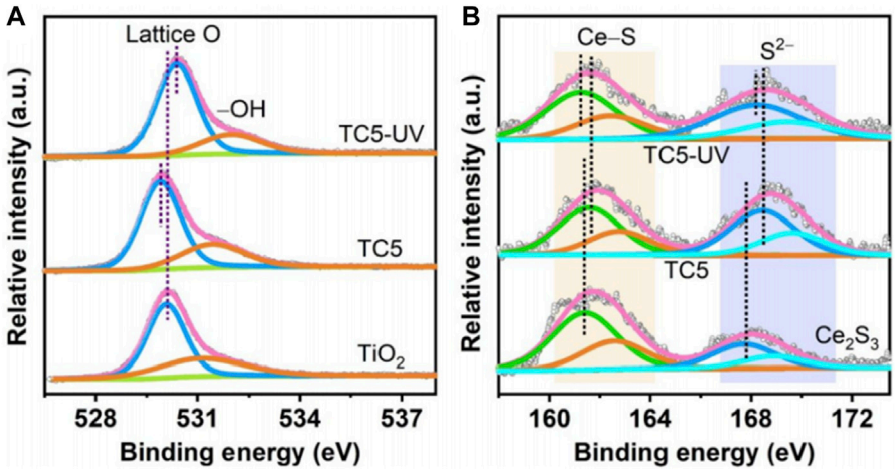

FIGURE 4
X-ray photoelectron spectroscopy (XPS) spectra of TC_X and reference catalysts. **(A)** O 1s of TiO_2 and TC5, and **(B)** S 2p of Ce_2S_3 and TC5. Reproduced with permission from reference (Xu et al., 2021).

rate of photogenerated electron hole pairs decreased significantly and the photogenerated electrons could be efficiently transferred from TiO_2 nanocrystals to heterogeneous Pt nanoparticles. As a result, in photocatalytic SHN, under the conditions of 50.0 mg catalyst, 50.0 mL nitrobenzene, 0.6 mL triethanolamine, room temperature and 300 W Xe lamp irradiation, after evaluating for 8.0 h, nitrobenzene conversion and the selectivity towards aniline were 44.0% and 99.0%, respectively. Further extending the reaction time to 20.0 h could boost nitrobenzene conversion and the selectivity towards aniline to 95.0% and 99.0%, respectively.

② Constructing a heterojunction photocatalyst with another semiconductor. A heterojunction is an interface region formed by the contact of two different semiconductors. Heterojunctions often exhibit excellent optoelectronic properties that cannot be achieved by the respective single semiconductors, which poses heterojunction an important position in the field of photocatalysis (Zhou et al., 2018; Ramezanalizadeh and Rafiee, 2020; Yang, 2021). Due to the inconsistency of VB, CB and BG energies, in heterojunctions, the overlap occurs, which promotes the separation of photogenerated electrons and holes, expands the spectral response of TiO_2, and exhibits better stability and catalytic activity in photocatalytic reactions (Yu et al., 2021; Xu et al., 2022; Zhao et al., 2022).

The research done by Xu et al. (2021) is a representative work. The authors successfully grew Ce_2S_3 nanoparticles on electrospun TiO_2 nanofibers by a solvothermal strategy (Xu et al., 2021). The resulting Ce_2S_3/TiO_2 heterojunction was named TC_X (T: TiO_2, C: Ce_2S_3, x: molar percentage of Ce_2S_3 in TC_X), which served as a photocatalyst for photocatalytic SHN, with water as a proton source. Performance evaluation results indicated that both TiO_2 nanofibers and Ce_2S_3 nanoparticles exhibited low aniline productivity, with aniline yields of 51.0% and 33.0%, respectively; on the contrary, TC_X were efficient for aniline production, with the yield of aniline reaching 99.0% when TC5 was used as catalyst under irradiation for 1.5 h. Characterization suggested that in TC5 catalyst, the binding energies of Ti 2p and O 1s were negatively shifted compared with TiO_2 (Figure 4A) and the binding energies of Ce 3d and S 2p of TC5 were shifted positively relative to that of Ce_2S_3 (Figure 4B), indicating that there was electron transfer from Ce_2S_3 to TiO_2 when they were combined without light irradiation. Such an

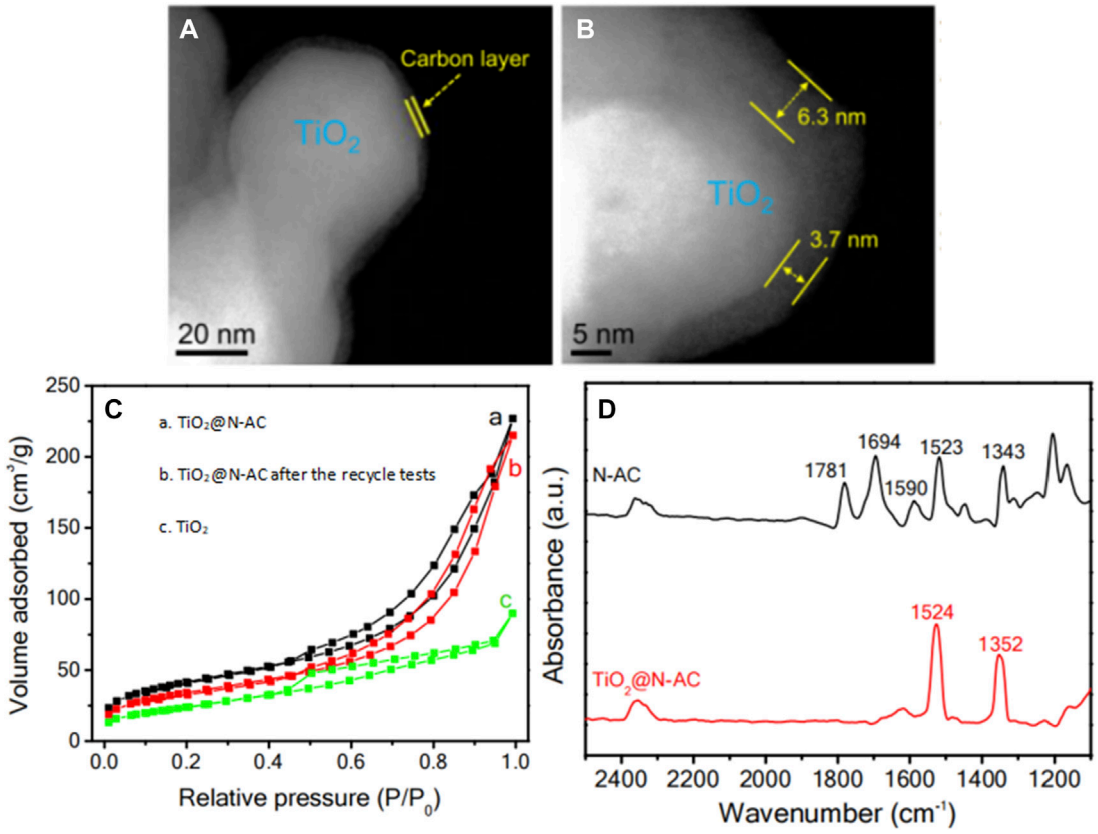

FIGURE 5
(A, B) HAADF-STEM images of TiO_2@N-AC, **(C)** N_2 adsorption-desorption isotherms, and **(D)** FTIR spectra of mixed nitrobenzene and benzaldehyde on TiO_2@N-AC and N-AC. Reproduced with permission from reference (Xu et al., 2019).

electron transfer between TiO_2 and Ce_2S_3 caused the internal electric field pointing from Ce_2S_3 to TiO_2. In the case that under light irradiation, the binding energies of Ti 2p and O 1s of TC5 were positively shifted, but the binding energies of Ce 3d and S 2p of TC5 were negatively shifted, which confirmed the migration of photoexcited electrons in TiO_2 CB into Ce_2S_3 VB under illumination. Meanwhile, the energy bands of TiO_2 and Ce_2S_3 bent at the interfaces, which drove the efficient separation of photogenerated charge carriers over Ce_2S_3/TiO_2 heterojunction and enhanced its photocatalytic performance.

③ Constructing a hybrid catalyst with non-semiconductor component. Hybrid catalysts generally contain active components with different catalytic functions (Prasad et al., 2020; Ahmad et al., 2023). Occasionally, an interface will be formed between the chemical components of the hybrid catalyst, which could improve the overall performance and stability (Han et al., 2018). In this regard, Xu et al. (2019) designed a TiO_2@N-AC hybrid catalyst, with TiO_2 as the core and nitrogen-doped carbon (N-AC) as the shell. The thickness of the carbon layers was in the range of 3.5–7.5 nm, evidenced by high-angle annular dark field-scanning transmission electron microscopy (HAADF-STEM) images in Figures 5A, B. Compared with bare TiO_2 (73 $m^2 g^{-1}$), TiO_2@N-AC had a large specific surface area (Figure 5C, 234 $m^2 g^{-1}$) and abundant mesopores, which facilitated the diffusion of reactant molecules to the surface of TiO_2 and enhanced the adsorption of nitrobenzene, making TiO_2@N-AC highly active and selective in the photocatalytic hydrogenation of nitrobenzene. Noteworthy, under the reaction conditions of 0.08 mmol nitrobenzene, 10.0 mg TiO_2@N-AC catalyst, 4.0 mL isopropanol, reaction temperature 30°C and reaction time 6.0 h, the conversion rate of nitrobenzene reached 99.1% and the selectivity towards aniline reached 98.8%. Moreover, TiO_2@N-AC also exhibited high conversion and selectivity towards the corresponding functionalized anilines in photocatalytic hydrogenation of nitroarenes with various substituents (such as -Cl, -F, -C=C, C=O, and -C≡N), even better than noble metal-based catalysts (such as Pt, Ag). *In-situ* fourier transform infrared (FTIR) spectrum only gave the band of nitro group when an equivalent amount of nitrobenzene and benzaldehyde were introduced into the TiO_2@N-AC catalyst (Figure 5D), confirming the unique characteristic of TiO_2@N-AC to selectively adsorb nitrobenzene, which explained the superior catalytic performance of TiO_2@N-AC in photocatalytic SHN.

2.2 CoS_2

As one of the representatives of transition metal disulfide, CoS_2 is considered as a potential photocatalyst due to its low cost, excellent electronic conductivity, thermal stability and photochemical properties (Ahmad et al., 2018; Tang et al., 2019; Zhang et al., 2022), which makes it applicable in photocatalytic SHN. However, the catalytic performance of

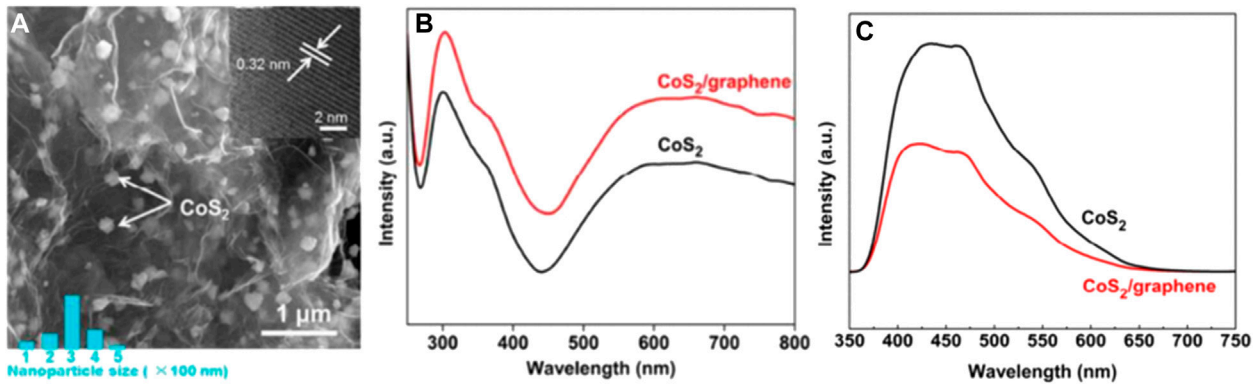

FIGURE 6
(A) Field emission scanning electron microscopy (FESEM) images of CoS_2/graphene, **(B)** UV-vis diffuse reflectance spectra, and **(C)** photoluminescence spectra of CoS_2 and CoS_2/graphene. Reproduced with permission from reference (Ma et al., 2017).

CoS_2 is not satisfactory (the conversions of nitrobenzene over CoS_2 were 72.0% under light irradiation and 23.0% without light irradiation) and needs further improvement (Ma et al., 2017).

Ma et al. (2017) study is a representative to improve the catalytic performance of CoS_2 in photocatalytic SHN. The authors prepared a CoS_2/graphene composite catalyst, by uniformly dispersing CoS_2 on the graphene sheets (Figure 6A), a material with high electrical conductivity, excellent electron mobility and high surface area. It revealed that, in photocatalytic SHN, over CoS_2/graphene, under the conditions of 40.0 mg catalyst, 1.0 mmol nitrobenzene, 10.0 mL ethanol, 30°C, 0.25 MPa H_2 and 300 W Xe lamp irradiation, after evaluating for 1.5 h, nitrobenzene conversion and the selectivity towards aniline reached 99.0% and 100.0%, respectively. Characterization results suggested that CoS_2/graphene exhibited better light harvesting efficiency, evidenced by the ultraviolet-visible (UV-visible) spectra in Figure 6B, where the absorption at 450–800 nm was attributed to the d-d transitions of Co(II) ions in CoS_2. Furthermore, when CoS_2 was supported on graphene, the photogenerated electrons in CoS_2 could quickly transfer to the conductive graphene sheet, thereby suppressing electron-hole recombination (Figure 6C). Moreover, graphene has a large specific surface area and rich pore structure, which provided more active sites for H_2 adsorption. According to the above characterization conclusion, it is reasonable to speculate that, on the one hand, H_2 can be activated by photoexcited holes on the surface of CoS_2 and form active hydrogen species; On the other hand, nitrobenzene molecules are adsorbed on the catalyst surface, and the N-O bond is also activated by photogenerated electrons; Finally, the active hydrogen species migrate to the surface of the active nitrobenzene molecule to form aniline. The improved light harvesting efficiency, suppressed electron-hole recombination rate together with the more available active sites, accounted for the better catalytic performance of CoS_2/graphene in photocatalytic SHN.

2.3 Ce_2S_3

Ce_2S_3 is a semiconductor with BG value of 2.1 eV, CB of −0.91 eV and VB of 1.19 eV, respectively (Xu and Schoonen, 2000; Ranjith et al., 2016; Xu et al., 2021; Jia et al., 2022; Rauf et al., 2022). The highly negative potential of CB allows Ce_2S_3 as an ideal photocatalyst for SHN (Kudo and Miseki, 2008). Chen et al. (2013) synthesized a Ce_2S_3 catalyst by the coprecipitation method, which realized a nitrobenzene conversion and a selectivity towards aniline of 36.2% and 43.9%, respectively, under the conditions of 0.56 g (4.0 g L^{-1}) catalyst, 30°C, 375 W mercury lamp irradiation and 5.0 h reaction time.

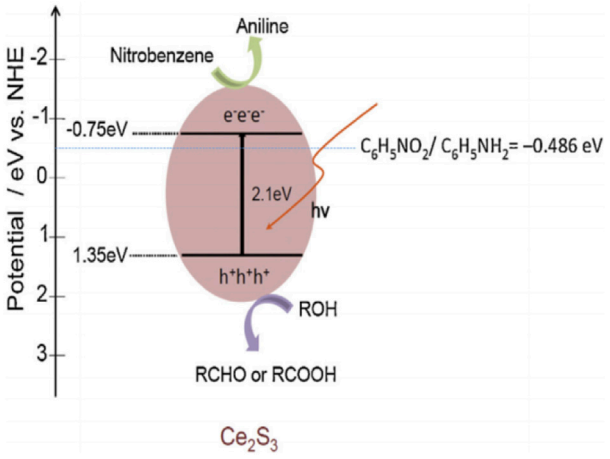

FIGURE 7
Mechanism of SHN catalyzed by Ce_2S_3 photocatalyst. Reproduced with permission from reference (Chen et al., 2013).

The evaluation conditions influence greatly on the performance of Ce_2S_3 in SHN. ① Catalyst concentration. When the catalyst concentration was lower than 4.0 g L^{-1}, the catalytic performance increased with the increasing of the photocatalyst dosage, owing to the improved utilization of photons; However, light scattering and shielding effects occurred when the catalyst concentration exceeded 4.0 g L^{-1}, which resulted in the ineffective utilization of Ce_2S_3 and photons. Therefore, the optimal catalyst concentration was

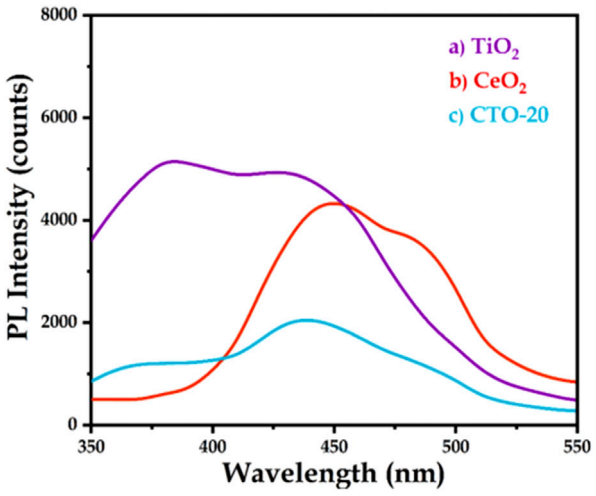

FIGURE 8
PL spectra of TiO_2, CTO-20, and CeO_2 nanomaterials.
Reproduced with permission from reference (Lu et al., 2021)

determined as 4.0 g L^{-1}. ② Hole scavenger. Methanol is a better hole scavenger than others (such as ethanol and isopropanol) because of its advantages, such as lower viscosity, higher polarity, lower polarizability as well as easier to be captured by photoexcited holes.

According to the energy band structure of Ce_2S_3 calculated by empirical equation (Eqs 1, 2), the approximate reaction mechanism is inferred (Figure 7).

$$E_{VB} = X - E_e + 0.5E_g \quad (1)$$

$$E_{CB} = E_{VB} - E_g \quad (2)$$

(where E_{VB} is the VB edge potential, X is the electronegativity of the semiconductor, E_e is the standard hydrogen electrode potential, and E_g is the BG energy of the semiconductor.)

The photocatalytic reduction of nitrobenzene occurs on the surface of Ce_2S_3, and photogenerated electron hole pairs will be generated under illumination. In order to prevent the recombination of electron hole pairs, methanol is adsorbed on the surface of Ce_2S_3 to capture holes to reduce the recombination rate, increase the probability of photoexcited electrons adsorbed on Ce_2S_3, and improve the conversion rate of nitrobenzene reduction to aniline (Figure 7).

2.4 CeO_2

The BG of CeO_2 is about 3.19 eV. In addition, CeO_2 has a dynamically reversible Ce^{3+}/Ce^{4+} redox site. It is one of the promising catalysts or promoters in hydrogenation of nitrobenzene, since it is beneficial for the adsorption of nitro groups on its surface (Huang et al., 2021). Based on this background, Lu et al. (2021) prepared CeO_2 modified TiO_2 nanocomposites by sol-gel method, and evaluated their performance in photocatalytic hydrogenation of nitrobenzene. It revealed that, CeO_2-TiO_2 (the weight ratio of CeO_2 was 20%, short for CTO-20) could realize a nitrobenzene conversion and a selectivity towards aniline of 98.0%, under the conditions of 20.0 mg catalyst, 1.0 mmol nitrobenzene, 2.0 mmol hydrazine hydrate, 4.0 mL methanol, 25°C, 300 W Xenon lamp irradiation and reaction time 4.0 h. Compared with pure TiO_2 and pure CeO_2, CTO-20 nanocomposites had a larger amount of oxygen vacancies, inhibited the combination of electron-hole pairs (Figure 8) and exhibited the highest catalytic activity. Characterization revealed that, the photogenerated electrons in the CB fell into the energy level of the oxygen vacancy through the non-irradiation process, and then recombined with the photogenerated holes in the VB, accompanied by fluorescence emission. Thus the recombination of the photogenerated carriers was suppressed. Based on the energy band structure of CeO_2 and TiO_2, the possible mechanism of hydrogenation of nitrobenzene under visible light was proposed: photogenerated electrons were excited to CB, leaving holes at VB of TiO_2, and photogenerated holes at VB of TiO_2 migrated to VB of CeO_2. Here, methanol in the reaction system acted as a hole scavenger, trapping the holes on CeO_2 VB, preventing the recombination of carriers. Therefore, the photogenerated holes of TiO_2 at VB has strong oxidation ability, which can effectively oxidize and split hydrazine hydrate into protons and electrons. Then nitrobenzene was reduced by electrons and protons at the CB of TiO_2, and aniline was obtained as the final product under visible light irradiation.

2.5 CdS

CdS has a bandgap of 2.4 eV and is strong in harvesting visible light (Jingrun et al., 2014; Yu et al., 2019; Li et al., 2020; Cui et al., 2021). However, as a photocatalyst, CdS suffers from the following disadvantages, ① the photogenerated electrons and holes recombine quickly, resulting in low quantum efficiency for solar light utilization, and ② the photostability of CdS is relatively poor (Zhang et al., 2011; Eskandari et al., 2014; Gao et al., 2015; Zhang et al., 2019a). To overcome the shortages of CdS, several heterojunction/hybrid catalysts have been designed.

Xiao et al. (2014) and Ye et al. (2017) studies are representatives. Xiao et al. (2014) constructed a graphene nanosheets-CdS quantum dots composite films and adopted it for the selective reduction of various halogenated nitroaromatic hydrocarbons under visible light conditions. Under the condition of 15.0 mL (10.0 mg L^{-1}) nitroaromatic, 20.0 mg HCO_2NH_4, 25°C and 300 W Xe lamp irradiation, after evaluating for 3.0 h, the conversion rate of various nitroaromatic substances (such as 1-chloro-4-nitrobenzene, 1-bromo-4-nitrobenzene and 4-nitrotoluene etc.) reached about 80.0%. The high activity was mainly due to the capture of photo-excited electrons by graphene nanosheets, which significantly enhanced the adsorption of substrates, facilitated electron hole separation and consequently increased the possibility of photo-induced electrons participating in photocatalytic hydrogenation. Ye et al. (2017) fabricated a CdS/graphitic carbon nitride (CdS/g-C_3N_4) heterostructure catalyst for SHN research. It revealed that, in photocatalytic SHN, over CdS/g-C_3N_4, under the conditions of 0.1 g catalyst, 15.0 mL benzotrifluoride solution (benzyl alcohol and nitrobenzene), 60°C and 300 W Xe lamp irradiation, after evaluating for 4.0 h, nitrobenzene conversion and the selectivity towards aniline reached 49.2% and 52.8%, respectively, much higher selectivity than those on CdS (18.0% and 37.5%, respectively) and g-C_3N_4 (11.0% and 40.0%, respectively). Characterization suggested that the edge of the absorption

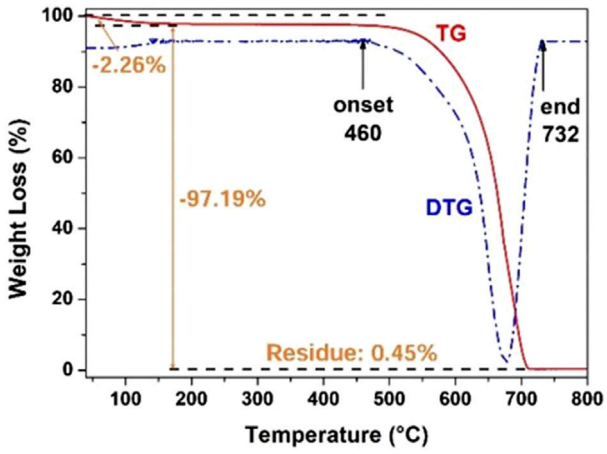

FIGURE 9
TG/DTG curves of the synthesized g-C_3N_4 catalyst in air. Reproduced with permission from reference (Xiao et al., 2018).

band of CdS/g-C_3N_4 was red-shifted compared with that of pure g-C_3N_4, which was beneficial for harnessing solar energy. Meanwhile, the introduction of g-C_3N_4 limits the growth of cadmium sulfide particles, resulting in a larger specific size and specific surface area of CdS/g-C_3N_4, which has higher catalytic activity. In addition, there was a strong interaction between CdS and g-C_3N_4, which was conducive to the efficient separation and migration of photoexcited carriers, thereby improving the photocatalytic activity.

2.6 g-C_3N_4

As a semiconductor, g-C_3N_4 has a unique electronic energy band and visible light activity with a BG of about 2.7 eV. In addition, g-C_3N_4 is non-toxic and cheap, with excellent physical and chemical stability (Ismael, 2020; Li et al., 2022a; Wudil et al., 2023). The merits of g-C_3N_4 make it as an excellent photocatalyst in visible light region. For example, Xiao et al. (2018) synthesized a polymerized g-C_3N_4 photocatalyst *via* thermally condensing urea at high temperatures. The polymerized g-C_3N_4 catalyst had a unique structure with a loose and porous sheet-like morphology, and specific surface area of 74.2 $m^2 g^{-1}$. In addition, thermogravimetric analysis (TGA) revealed an onset temperature of g-C_3N_4 pyrolysis as high as 460°C (Figure 9), indicating that the synthesized g-C_3N_4 had excellent chemical stability in air at temperatures lower than 460°C. In photocatalytic SHN, over g-C_3N_4, under the conditions of 20.0 mg catalyst, 0.2 mmol nitrobenzene, 2.0 mL H_2O, 1.0 mmol hydrazine hydrate, 90°C and 300 W Xe lamp irradiation, after evaluating for 20.0 h, nitrobenzene conversion and the selectivity towards aniline reached 100.0% and >99.0%, respectively. Mechanism study indicated that, when the transient electron hole pair was generated on the g-C_3N_4 surface upon light irradiation, the generated photoelectrons were transferred to the nitrobenzene molecules adsorbed on g-C_3N_4, and hydrazine (a strong reducing agent) effectively removed the holes, thus strengthening the segregation of charge carriers and accelerating the hydrogenation of nitrobenzene to aniline.

2.7 Polymeric carbon nitride (PCN)

PCN has the advantages of easy synthesis, visible light sensitivity and suitable energy bands. During the past few years, it has been successfully used in the hydrogenation of nitrobenzene (Wang et al., 2018a; Liao et al., 2021; Patel et al., 2021). Generally speaking, pristine PCN exhibits poor catalytic activity and modification is necessary to achieve high catalytic performance.

For instance, Pei et al. (2021) designed a surface -OH group-modified PCN (denoted as PCN-160, since it was treated at 160°C) *via* a simple green hydrothermal treatment method, which could realize a nitrobenzene conversion and a selectivity towards N-phenylhydroxylamine (PHA) of 98.0% and 80.0%, under the conditions of 50.0 mg catalyst, 30.0 μmol nitrobenzene, 1.5 mL isopropanol, 60°C, 100 W white light emitting diode (LED) lamp irradiation and reaction time 18.0 h. DFT calculations showed that the interaction energies of PHA and nitrobenzene were 0.57 eV and 0.40 eV on PCN. Through the hydrogen bonding interaction, PCN-160 energy was enhanced by 0.12 eV and 0.42 eV, respectively. In PCN-160, the O—H···O hydrogen bond replaced the O—H···N hydrogen bond, where the bond length of O—H···O was shorter than O—H···N. The significant change in energy and a decrease in hydrogen bond length (from 2.110 to 1.893 Å, 1.963 to 1.782 Å) between nitrobenzene and the active center -OH favored the hydrogenation of nitrobenzene (Figures 10A–D). Over PCN-160, ① the introduction of -OH functional groups shifted the CB of PCN to a suitable position, thus reducing the recombination probability during electron transfer and providing high-energy photogenerated electrons to promote the reduction of nitrobenzene; and ② the introduced -OH groups facilitated the adsorption of nitrobenzene, reduced the recombination velocity of electron hole pairs, and provided a large number of protons to participate in the hydrogen transfer process. The above two factors worked synergistically to achieve the cumulation of PHA and ensure high selectivity of the reaction (Figure 10E).

2.8 Metal-organic frameworks (MOFs)

MOFs are a kind of coordination polymers, which have burgeoned in recent decades and are extensively served as catalysts. MOFs have a three-dimensional pore structure, in which metal ions are generally used as attachment points to support organic ligands to form spatial 3D extensions (Wang et al., 2017; Amarajothi et al., 2018; Zhang et al., 2019b; Li et al., 2022b). The MOFs' crystal dimensions, conformation, and crystal texture can significantly tailor the visible light absorption capacity, charge separation efficiency, and directional electric charge transport (Kouser et al., 2023).

Cheng et al. (2020) study is representative for the application of MOFs in photocatalytic SHN. They embedded Pd nanoparticles in the cavities of assorted Fe-MOFs (MIL-101(Fe)-2MI, NH_2-MIL-101(Fe)-2MI and etc.) *via* impregnation method and calcined them in nitrogen to form "quasi-MOF" catalysts (Pd/MIL-101(Fe)-2MI(300), Pd/NH_2-MIL-101(Fe)-2MI(300), etc., (where "300" represents the calcination temperature). Over Pd/NH_2-MIL-101(Fe)-2MI(300), under the conditions of 0.1 mmol% catalyst, 0.1 mmol nitrobenzene, 3.0 mmol benzyl alcohol, 2.0 mL CH_3CN and 0.75 W cm^{-2} blue LED irradiation, after evaluating for 24.0 h,

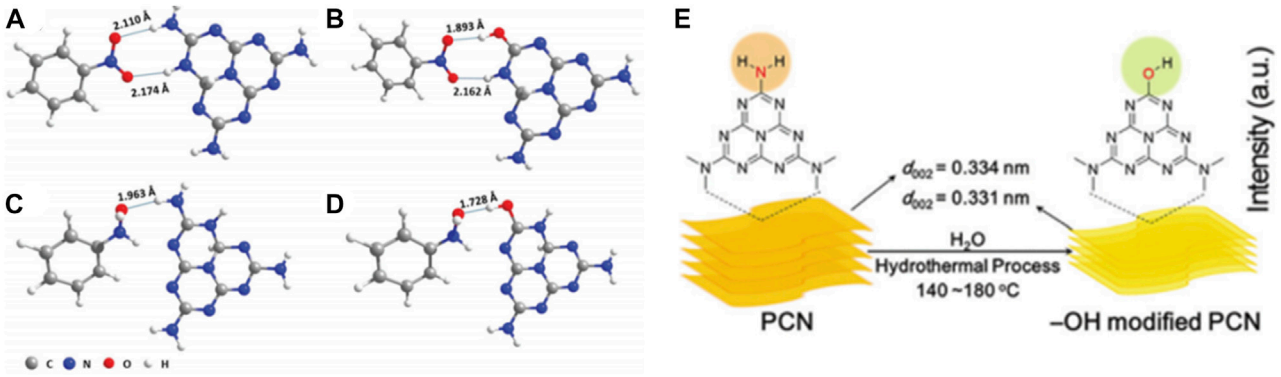

FIGURE 10
Reaction mechanism model diagram. **(A, C)** The best adsorption states of nitrobenzene and PHA on PCN, **(B, D)** the best adsorption states of PCN modified by -OH for nitrobenzene and PHA (where the numbers indicate the length of hydrogen bond), and **(E)** schematic diagram of hydroxyl modified PCN. Reproduced with permission from reference (Pei et al., 2021).

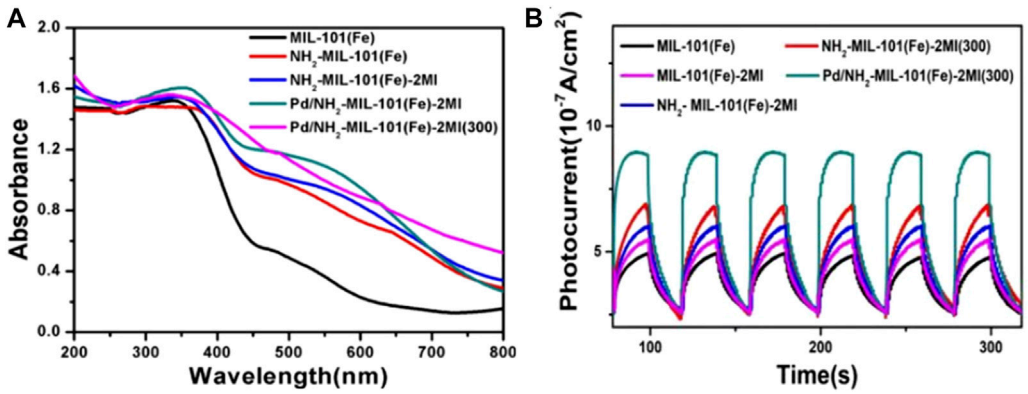

FIGURE 11
MOF and Pd/MOF catalysts. **(A)** UV-Vis diffuse reflectance spectra, and **(B)** photocurrent response. Reproduced with permission from reference (Cheng et al., 2020).

nitrobenzene conversion and the selectivity towards N-benzyl aniline reached 100.0% and 85.0%, respectively (Cheng et al., 2020). UV-vis diffuse reflectance spectra (Figure 11A) suggested that all the catalysts were capable for harvesting visible light, which proved their feasibility as photocatalysts. In addition, Pd/NH_2-MIL-101(Fe)-2MI(300) with amino groups, 2MI and the loading of Pd nanoparticles, exhibited the highest photocurrent (Figure 11B), indicating supreme charge transfer efficiency and minimum charge transfer electric resistance. The light harvesting capacity as well as the highest photocurrent responded for the high catalytic performance of Pd/NH_2-MIL-101(Fe)-2MI(300).

3 Plasmonic-metal based catalysts

Plasmonic-metal based photocatalysts with localized surface plasmon resonance (LSPR) effects are gradually emerging because of their capacity to harness an ultra-wide spectrum of sunlight. LSPR is a physical optical phenomenon. It uses the evanescent wave that penetrates the metallic membrane when the light is fully reflected at the interface between the glass and the metal film, which induces free electrons in the metal to generate surface plasmons (Xie et al., 2022). LSPR effect mainly exists in plasmonic metals, such as Au, Cu and Ag (Zheng et al., 2014; Kavitha and Kumar, 2019; Wang et al., 2021; Silva et al., 2022). Efficiently identifying and directing energy pathways from the plasmonic metals to substrates is considered a key to achieve improved catalytic efficiency (Gellé and Moores, 2019; Silva et al., 2022). In this subsection, we will describe the applications of plasmonic-metal based catalysts in photocatalytic SHN.

3.1 Au-based catalysts

Huang et al. (2021) investigated the feasibility of Au-based catalysts in photocatalytic SHN. They prepared a series of Au/ZrO_2 catalysts with different Au loadings (1.5, 3.0, and 5.0 wt%) by supporting Au nanoparticles on ZrO_2 powder (Zhu et al., 2010).

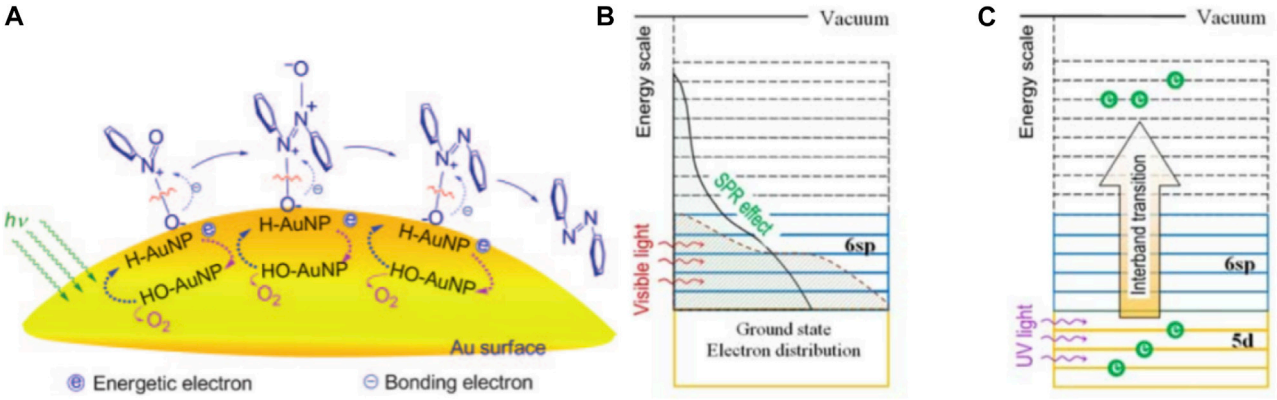

FIGURE 12
(A) Mechanism for the photocatalytic SHN over Au/ZrO_2, **(B)** electron excitation in Au nanoparticles due to the LSPR effect when illuminated with visible light, and **(C)** an interband transition when illuminated with UV light. Reproduced with permission from reference (Zhu et al., 2010).

It revealed that, in photocatalytic SHN, under the conditions of 100.0 mg catalyst, 3.0 mmol nitrobenzene, 30.0 mL isopropyl alcohol, 0.3 mmol KOH and 40°C, after evaluating for 5.0 h, 3.0% Au/ZrO_2 gave a nitrobenzene conversion of 100.0% and a selectivity towards azobenzene of >99.0%, respectively, much more active than 1.5% Au/ZrO_2 (59.0% and 88.0%, respectively) and 5.0% Au/ZrO_2 (69.0% and 82.0%, respectively). 1.5% Au/ZrO_2 was inferior owing to the less available active sites. On the other hand, over 5.0% Au/ZrO_2, the excessive Au loading led to the aggregation of Au nanoparticles and reduced the specific surface area of Au nanoparticles, where the catalytic reaction took place. In photocatalytic SHN, H-Au species were formed on the surface of Au nanoparticles, which were able to combine with the oxygen atoms of the N—O bond to generate HO-Au and achieve electrophilic N—O bond cleavage. Au nanoparticles absorbed visible light through the LSPR effect, resulting in changes of the electron distribution across energy levels and providing energy to cleave the N—O bond (Figure 12A). E.g., Au 6 sp electrons could gain energy through LSPR effect and migrate to higher energy levels (Figure 12B) and high-energy electrons could also be generated through electron interband excitation from Au 5d to Au 6 sp under UV light irradiation (Figure 12C).

3.2 Ag-based catalysts

Plasmonic properties of Ag endow Ag-based catalysts unique catalytic properties with high performance in various catalytic reactions (Wang et al., 2018b; Chaudhary and Ingole, 2018; Ojha et al., 2021; Zhao et al., 2021; Dutta et al., 2022; Shi et al., 2022). Ag-based catalysts have also been successfully applied in photocatalytic SHN. For instance, by taking advantages of the plasmonic properties of Ag as well as the high thermal and physicochemical stability of n-type semiconductor WO_3, Li et al. prepared WO_3-Ag nanowires by facial chemical method, where WO_3-Ag was formed by connecting massive WO_3 nanowires and slende Ag nanowires, with a multi-aperture network structure (Li et al., 2015). In photocatalytic SHN, under the conditions of 50.0 mg catalyst, 50.0 mL nitrobenzene-methanol solution, after evaluating for 2.0 h, WO_3-Ag gave a nitrobenzene conversion of 94.0%, which was much better than other catalysts (Ag and WO_3). WO_3 nanowires and WO_3-Ag nanowires exhibited similar isotherms with H_3-type hysteresis loops (Figure 13A). By comparison, WO_3-Ag exhibited a large specific surface area (77.1 $m^2\,g^{-1}$) while the specific surface area of WO_3 was 29.9 $m^2\,g^{-1}$. It indicated that the addition of Ag greatly increased the specific surface area of WO_3, which offered more active sites and promoted the photocatalytic reaction. In WO_3-Ag photocatalyst, Ag is a plasmonic metal. Ag can expand the light absorption to a longer wavelength and excite the electron-hole pairs in WO_3 by transferring the plasmon energy. Moreover, the energy of electrons or holes is transferred from plasmonic metal Ag to semiconductor with energy lower than the BG. The physical and chemical properties of the catalyst change, thus improving the activity and stability of the catalyst. Moreover, WO_3-Ag nanowires still remained more than 90.0% of the initial activity after four cycles. The spectra before and after cycling suggested that the catalyst structure remained basically unchanged, further confirming the structural stability of WO_3-Ag (Figure 13B).

3.3 Cu-based catalysts

Au- and Ag- based catalysts are the most extensively studied noble metal catalysts in photocatalytic reactions. Unfortunately, the high cost of Au and Ag seriously hindered the realization of industrial production. On the contrary, non-precious Cu-based catalysts exhibit excellent LSPR effects and have great potential to replace noble metals in photocatalytic reactions (Araújo et al., 2019; Xin et al., 2021).

Cu nanoparticles are of poor chemical stability, because they readily oxidize to CuO or Cu_2O in air or in the presence of trace amounts O_2. Guo et al. (2014) found that the electronic structure of Cu atoms on graphene could be affected by carbon vacancies and

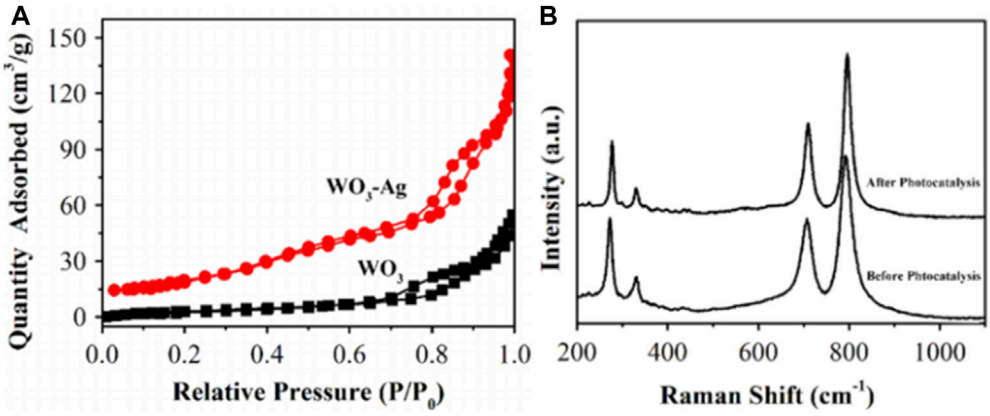

FIGURE 13
(A) N_2 adsorption-desorption isotherms of WO_3 nanowires and WO_3-Ag, and **(B)** Raman spectrum of WO_3-Ag before and after stability test. Reproduced with permission from reference (Li et al., 2015).

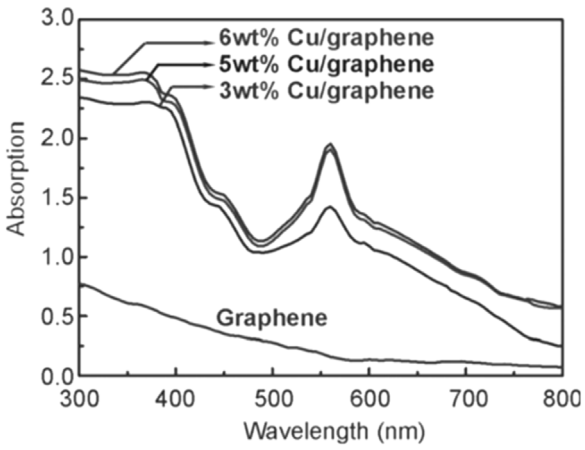

FIGURE 14
UV-vis absorption spectra of Cu/graphene photocatalysts. Reproduced with permission from reference (Guo et al., 2014).

dangling bonds in graphene, and ameliorated its chemical stability. Based on this discovery, they prepared a series of Cu/graphene catalysts with different Cu loadings (3.0, 5.0, and 6.0 wt%) for SHN. It revealed that, in photocatalytic SHN, under the conditions of 100.0 mg catalyst, 3.0 mmol nitrobenzene, 30.0 mL isopropyl alcohol, 0.3 mmol KOH, 300 W Xe lamp irradiation and 90°C, after evaluating for 5.0 h, 5.0% Cu/graphene gave a nitrobenzene conversion of 98.0% and a selectivity towards azobenzene of 98.0%, respectively, much more active than 3.0% Cu/graphene and 6.0% Cu/graphene. 3.0% Cu/graphene exhibited significantly weaker LSPR absorption due to the low content of Cu (Figure 14). The Cu particles in 6.0% Cu/graphene (40.3 nm) were much larger than those in 5.0% Cu/graphene (15.4 nm), which resulted in smaller specific surface area and fewer active centers than 5.0% Cu/graphene. In photocatalytic SHN, isopropanol acted as a hydrogen source and reaction solvent, and KOH enhanced the hydrogen release of isopropanol. The released hydrogen bonds formed H-Cu species on Cu surfaces, which produced HO-Cu by trapping oxygen atoms in N-O bonds, resulting in azobenzene. The high-energy electrons excited by the Cu LSPR effect strongly interacted with the electrophilic nitro group in the nitrobenzene, which promoted the cleavage of the N-O bond and accelerated the reaction.

In addition to metallic Cu, chalcopyrite ($CuFeS_2$), which is a natural mineral, exhibits LSPR properties (Bhattacharyya and Pandey, 2016; Ghosh et al., 2016; Sugathan et al., 2018). Poulose et al. (2022) adopted sunlight as the only energy input, $CuFeS_2$ as the catalyst, and hydrazine as the solvent to provide protons and electrons for photocatalytic SHN. Over $CuFeS_2$, under the conditions of 10.0 mg catalyst, 0.1 mmol nitrobenzene, 0.8 mL hydrazine, 3.0 mmol ethanol and room temperature, after evaluating for 2.0 h, both the conversion of nitrobenzene and the selectivity to aniline reached 100.0%. When the reaction was carried out at 40°C without light irradiation, the yield of aniline reached 44.1%, indicating the intrinsic activity of $CuFeS_2$ was mainly stemmed from the photocatalytic process. Transient absorption spectroscopy (TAS) study revealed two main processes (Wang et al., 2015), photoinduced absorption (PIA) and (Maji et al., 2011) photobleaching (PB) features, respectively (Figures 15A, B). The PIA curve and PB feature observed at the same time was attributed to the transition from the temporary occupation state in the median to CB, and the transition from depleted VB to the state in the median, respectively. Among them, the excess energy of carrier cooling excited electrons was transferred to the lattice, which eventually led to the heating of nanocrystals. It indicated the formation of holes in the VB of $CuFeS_2$ and hot electrons was formed in the intermediate band and CB of $CuFeS_2$ (Figure 15C). This energy matching promoted the good interaction between the highest occupied molecular orbital of hydrazine and the VB holes of $CuFeS_2$, which was considered as the main reason for the excellent performance of $CuFeS_2$. In addition, there was synergy between the metal centers, Fe and Cu in $CuFeS_2$. Fe central site was used to bind and activate hydrazine to form instantaneous spin active species, $[H(FeS_2)NH\text{-}NH_2]$, which delivered protons and electrons to the

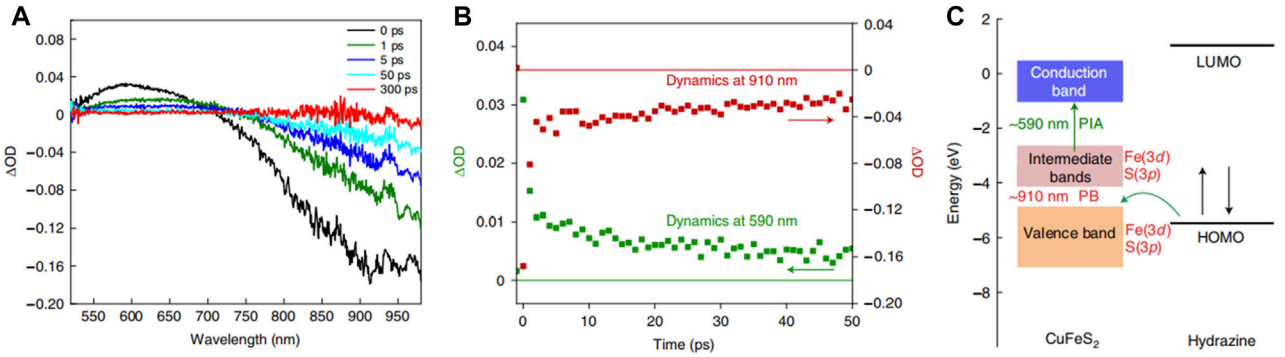

FIGURE 15
(A) Time-resolved TAS of $CuFeS_2$ catalysts, **(B)** the transient dynamics of $CuFeS_2$ PIA at 590 nm and PB at 910 nm, and **(C)** diagrammatic sketch of energy level diagrams of $CuFeS_2$ and hydrazine. Reproduced with permission from reference (Poulose et al., 2022).

adjacent $Cu(I)S_2$ site. $Cu(I)S_2$ sites interacted with the nitro-substrate to produce the N-phenylhydroxylamine radical. For these reasons, $CuFeS_2$ can not only form optical excitation complexes with the reactants but also possess a particularly high reaction rate.

4 Dye as photocatalyst

Organic dyes produce excited states by absorbing visible light and making transitions (dye*). Then electrons transfer to dye* to form $dye^{+\cdot}$ radical and reactant radical anion. After that, reactant radial anion is reduced to the target product and dye is regenerated from $dye^{+\cdot}$ radical by scavenger. A key feature of dye as photocatalyst is that their energy levels (i.e., highest occupied molecular orbital) are more flexible and tunable (Zhang and Zhu, 2005; Lang et al., 2014; Franchi and Amara, 2020; Yang et al., 2022). Therefore, dye-catalyzed systems are promising for photocatalytic SHN.

Eosin Y (EY) is a chemically synthesized acid dye and has been widely utilized as catalyst due to its simple structure, low price, and good effect (Liu et al., 2020; Dhara et al., 2021). For instance, Yang et al. (2014) reported a simple and efficient catalytic hydrogenation reduction reaction of nitrobenzene with EY as catalyst and triethanolamine (TEOA) as reducing agent under the illumination of green LED light. Under the conditions of EY (1.0 mol%) catalyst, 0.2 mmol nitrobenzene, $EtOH/H_2O$ (3:2) of 5.0 mL, pH 8.5 and room temperature, after evaluating for 8.0 h, nitrobenzene conversion and the selectivity towards aniline reached 100.0% and 93.0%, respectively. The absorption peak of λ_{max} at 270 nm is the absorption of light by nitrobenzene, which gradually decreases with time. The absorption peak of λ_{max} at 240 nm is the absorption of light by aniline. The transfer of the peak indicates that nitrobenzene is successfully converted into aniline. In the photocatalytic reaction, the position of the absorption peak and the intensity of λ_{max} at 520 nm remained almost unchanged, which indicated that EY was very stable (Figure 16). It may be due to the formation of EY cationic radicals ($EY^{+\cdot}$), which makes the electron transfer from TEOA to $EY^{+\cdot}$, and leads to the rapid regeneration of EY. After a series of control experiments, it was found that there were two important factors affecting the photocatalytic performance

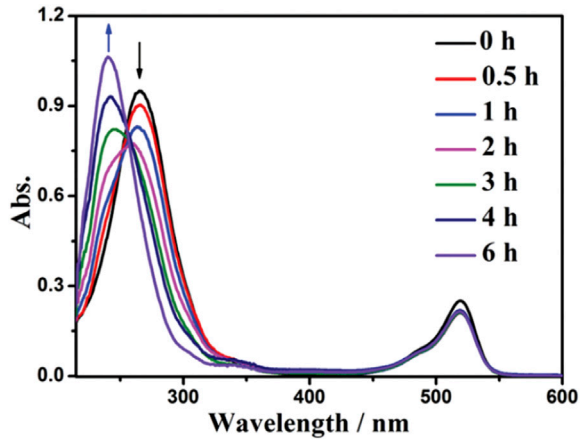

FIGURE 16
Changes of UV-vis absorption spectrum of nitrobenzene solution during irradiation. Reproduced with permission from (Yang et al., 2014).

of EY in SHN. ① The pH range of the catalytic system. In this photocatalytic system, the optimal pH range was about 8.5, TEOA acted as a sacrificial electron donor, providing electrons and protons for reduction reactions. In strong alkaline solutions, the reduction efficiency was very low since a limited number of protons was available for the reduction process. On the contrary, in strong acid solution, TEOA would be protonated, thereby reducing its electron donation ability and efficiency. ② The dosage of TEOA. In the reduction process, each TEOA molecule can contribute two electrons and two protons. Therefore, when three equivalent TEOA was used, full conversion can be achieved. The mechanism on photocatalytic SHN by EY was proposed. For the photoinduced electron transfer from the triplet EY to nitrobenzene in the charge transfer route, $EY^{+\cdot}$ and nitrobenzene radical anions will be formed. At the same time, the electron transfer from TEOA to $EY^{+\cdot}$ will regenerate EY and give $TEOA^{+\cdot}$, and then the nitrobenzene radical anion reacts with TEOA to finally produce aniline.

TABLE 1 The performance of some typical catalysts in SHN reaction.

Catalysts	Catalyst type	Reaction conditions	Product yield (%)	Ref.
Rutile TiO_2	Semiconductor	Catalyst: 5.0 mg, 2-PrOH: 5.0 mL, nitrobenzene: 10.0 mmol, illumination: 500 W, λ > 300 nm, Xe lamp.	97.0	Shiraishi et al. (2012)
TiO_2@N-AC	Semiconductor	Catalyst: 10.0 mg, nitrobenzene: 0.08 mmol, isopropanol: 4 mL, temperature: 30°C, irradiation: 300W, λ > 350 nm, Xe lamp, reaction time: 6.0 h	98.8	Xu et al. (2019)
Pt-TiO_2-RGO	Semiconductor	Catalyst: 50.0 mg, nitrobenzene: 50.0 mL, triethanolamine: 0.6 mL, room temperature, illumination: 300 W Xe lamp irradiation, reaction time: 20.0 h	99.0	Qiu et al. (2016)
CoS_2/graphene	Semiconductor	Catalyst: 40.0 mg, nitrobenzene: 1.0 mmol, ethanol: 10.0 mL, temperature: 30°C, 0.25 MPa H_2, illumination: 300 W Xe lamp, reaction time: 1.5 h	100.0	Ma et al. (2017)
Ce_2S_3	Semiconductor	Catalyst: 0.56 g (4.0 g L^{-1}), 140 mL 8.13 × 10^{-4} mol L^{-1} of nitrobenzene in methanol solvent, illumination: 375 W Xe lamp, reaction time: 5.0 h	43.9	Chen et al. (2013)
CdS/g-C_3N_4	Semiconductor	Catalyst: 0.1 g, benzotrifluoride solution (benzyl alcohol and nitrobenzene): 15.0 mL, temperature: 60°C, illumination: 300 W Xe lamp, reaction time: 4.0 h	52.8	Ye et al. (2017)
g-C_3N_4	Semiconductor	Catalyst: 20.0 mg, nitrobenzene: 0.2 mmol, H_2O: 2.0 mL, hydrazine hydrate: 1.0 mmol, temperature: 90°C, illumination: 300 W Xe lamp, reaction time: 20.0 h	99.0	Xiao et al. (2018)
PCN	Semiconductor	Catalyst: 50.0 mg, nitrobenzene: 30.0 μmol, N-Phenylhydroxylamine: 1.5 mL, illumination: 100 W white LED lamp (0.6 Wcm^{-2}), temperature: 60°C, reaction time: 18.0 h	80.0	Pei et al. (2021)
Pd/NH_2-MIL-101(Fe)-2MI(300)	Semiconductor	Catalyst: 0.1 mmol% (based on Pd), nitrobenzene: 0.1 mmol, benzyl alcohol: 3.0 mmol, CH_3CN: 2.0 mL, illumination: 0.75 W cm^{-2} blue LED, reaction time: 24.0 h	85.0	Cheng et al. (2020)
Au/ZrO_2	Plasmonic-metal based catalyst	Catalyst: 100.0 mg, nitrobenzene: 3.0 mmol, isopropyl alcohol: 30.0 mL, KOH: 0.3 mmol, temperature: 40°C, reaction time: 5.0 h	99.0	Zhu et al. (2010)
Cu/graphene	Plasmonic-metal based catalyst	Catalyst: 100.0 mg, nitrobenzene: 3.0 mmol, isopropyl alcohol: 30.0 mL, KOH: 0.3 mmol, illumination: 300 W Xe lamp, temperature: 90°C, reaction time: 5.0 h	98.0	Guo et al. (2014)
$CuFeS_2$	Plasmonic-metal based catalyst	Catalyst: 10.0 mg, nitrobenzene: 0.1 mmol, hydrazine: 0.8 mL, ethanol: 3.0 mmol, room temperature, reaction time: 2.0 h	100.0	Poulose et al. (2022)
EY	Dye as catalyst	Catalyst: EY (1.0 mol%), nitrobenzene: 0.2 mmol, EtOH/H_2O (3:2): 5.0 mL, pH 8.5, room temperature, reaction time: 8.0 h	93.0	Yang et al. (2014)

5 Summary and outlooks

In the past few years, researchers have carried out extensive research in order to find efficient photocatalysts for SHN. Semiconductor, plasmonic metal-based catalyst and dye have been reported active in SHN. This paper summarizes the research progress of various catalysts for SHN, with special attention on semiconductor-based catalysts. Table 1 lists the performance of some typical catalysts.

In conclusion, the catalyst development is still in the initial stage, which is both an opportunity and a challenge, and huge difficulties need to be overcome.

(1) Selective hydrogenation of nitro group is challenging when other functional groups are present in the reactant nitroaromatics. Generally speaking, the hydrogenation reaction preferentially occurs on the thermodynamically more favorable functional group, or multiple unsaturated groups are hydrogenated at the same time, and the degree of hydrogenation cannot be precisely and finely controlled, making it difficult to control specific intermediates and by-products such as hydroxyaniline or azobenzene compounds are occasionally generated. Selective synthesis of hydrogenated products is very difficult, especially to selectively control the reaction pathways to aniline at present. Optimal reaction conditions could inhibit the occurrence of side reactions. For example, increasing the hydrogen pressure could inhibit the desorption of hydroxyaniline and lead it further hydrogenate to aniline, which could avoid the formation of hydroxyaniline as a by-product. Similarly, low reaction temperature can suppress the formation of azobenzene.

(2) An increase in activity is often accompanied by a decrease in selectivity, thus, it is challenging to realize high activity and high selectivity simultaneously. In this regard, there are still difficulties that have not been overcome for most catalysts. Compared with selectivity, conversion can be corrected by increasing process parameters (such as time and temperature), and selectivity promotion is more difficult and important. Future research needs to focus on in-depth study of the structure and distribution of catalyst active centers, increase the contact area between reactants and catalysts, reduce the occurrence of side reactions, and control the concentration gradient of reactants and the reaction at the kinetic level. Reasonable reaction conditions should be explored and suitable catalysts should be designed.

(3) Although noble metals, such as Au, Pt, and Pd, exhibit good catalytic activity, they cannot be applied in a large scale in industry due to their high cost. Therefore, the search for low-cost and high-performance catalysts has become an inevitable trend. In the follow-up research, under the premise of maintaining good conversion effect, it is necessary to focus on the development of new catalysts with simple preparation, low price, good stability and high activity.

(4) Most catalysts exhibit good performance under UV light irradiation, but they are not ideal under visible light irradiation. Therefore, enhancing the light harvesting capacities and widening the light absorption spectrum of the catalysts will be the focus of future research on photocatalytic SHN reaction. Transition metal complex catalysts and organic highly conjugated catalysts could be excited by visible light and exhibit high efficiency for light absorption, which might be the focus of catalyst development for photocatalytic SHN in the future.

(5) The reaction mechanism and corresponding active sites for the adsorption of reactants, dissociation of hydrogen, and subsequent stepwise hydrogenation remain controversial. More research is needed to focus on catalytic process analysis, with advanced and appropriate instrumentation, innovative work, extensive data studies, etc. For example, *in situ* attenuated total reflection infrared spectroscopy could be used to demonstrate the adsorption of substrates in each step of the hydrogenation reactions; with the assistance of theoretical calculations, TAS can be adopted to deduce the reaction mechanism.

(6) As a hydrogen source, alcohols can realize the equal synergistic conversion of nitrobenzene and alcohol under mild conditions. For example, when glycerol is used as the hydrogen source, it is efficiently converted into high value-added product 1,3-dihydroxyacetone during the synthesis of aniline. In addition, polyols, such as 1,3-propanediol, monosaccharide glucose and fructose can also be directly used as hydrogen sources to reduce nitrobenzene. It provides a new idea for the conversion of biomass to high-value-added fine chemicals.

Author contributions

JG, draft writing; HL, supervision; YL, figure editing; DL, language polishing; DH, polish and final review.

Funding

This work received financial support from the National Natural Science Foundation of China (21902116) and Scientific Research Foundation of Technology Department of Liaoning province of China (2022-MS-379).

Conflict of interest

The authors declare that the research was conducted in the absence of any commercial or financial relationships that could be construed as a potential conflict of interest.

Publisher's note

References

Abdullah, H., Gultom, N. S., Shuwanto, H., Kebede, W. L., and Kuo, D. H. (2020). Self-protonated HO-doped Zn(O,S) as a green chemical-conversion catalyst to hydrogenate nitro to amino compounds. *ACS Appl. Mater. Interfaces* 12 (39), 43761–43770. doi:10.1021/acsami.0c12695

Ahmad, I., Zou, Y., Yan, J., Liu, Y., Shukrullah, S., Naz, M. Y., et al. (2023). Semiconductor photocatalysts: A critical review highlighting the various strategies to boost the photocatalytic performances for diverse applications. *Adv. Colloid Interface Sci.* 311, 102830. doi:10.1016/j.cis.2022.102830

Ahmad, K. A., Sunita, K., Arif, C., and Sahid, H. (2018). Phase tuned originated dual properties of cobalt sulfide nanostructures as photocatalyst and adsorbent for removal of dye pollutants. *ACS Appl. Nano Mater.* 1 (7), 3474–3485. doi:10.1021/acsanm.8b00656

Akhundi, A., Moshfegh, A. Z., Habibi-Yangjeh, A., and Sillanp, M. (2022). Simultaneous dual-functional photocatalysis by g-C_3N_4-based nanostructures. *ACS ES&T Eng.* 2 (4), 564–585. doi:10.1021/acsestengg.1c00346

Aljahdali, M. S., Amin, M. S., and Mohamed, R. M. (2017). Gd-cobalt selenite as an efficient nanocomposite for aniline synthesis from photocatalytic reduction of nitrobenzene. *Mater. Res. Bull.* 99, 161–167. doi:10.1016/j.materresbull.2017.11.003

Amarajothi, D., Zhaohui, L., and Hermenegildo, G. (2018). Catalysis and photocatalysis by metal organic frameworks. *Chem. Soc. Rev.* 47, 8134–8172. doi:10.1039/c8cs00256h

Araújo, T. P., Quiroz, J., Barbosa, E. M., and Camargo, P. H. C. (2019). Understanding plasmonic catalysis with controlled nanomaterials based on catalytic and plasmonic metals. *Curr. Opin. Colloid & Interface Sci.* 39, 110–122. doi:10.1016/j.cocis.2019.01.014

Bhattacharyya, B., and Pandey, A. (2016). $CuFeS_2$ quantum dots and highly luminescent $CuFeS_2$ based core/shell structures: Synthesis, tunability, and photophysics. *J. Am. Chem. Soc.* 138 (32), 10207–10213. doi:10.1021/jacs.6b04981

Buzzetti, L., Crisenza, G. E. M., and Melchiorre, P. (2019). Mechanistic studies in photocatalysis. *Angew. Chem. Int. Ed.* 58 (12), 3730–3747. doi:10.1002/anie.201809984

Chaturvedi, R., and Singh, P. K. (2021). Synthesis and characterization of nano crystalline nitrogen doped titanium dioxide. *Mater. Today Proc.* 45 (5), 3666–3669. doi:10.1016/j.matpr.2021.01.276

Chaudhary, P., and Ingole, P. P. (2018). Multifunctional plasmonic Ag-hematite nano-dendrite electro-catalysts for methanol assisted water splitting: Synergism between silver nanoparticles and hematite dendrites. *Int. J. Hydrogen Energy* 43 (3), 1344–1354. doi:10.1016/j.ijhydene.2017.10.136

Chen, J., Na, Y., Wang, R., and Zhang, J. (2009). Hydrogenation of chloronitrobenzene to chloroaniline over Ni/TiO_2 catalysts prepared by sol-gel method. *Chem. Eng. J.* 148 (1), 164–172. doi:10.1016/j.cej.2008.11.046

Chen, P., Khetan, A., Yang, F., Migunov, V., Weide, P., Stürmer, S. P., et al. (2017). Experimental and theoretical understanding of nitrogen-doping-induced strong metal-support interactions in Pd/TiO_2 catalysts for nitrobenzene hydrogenation. *ACS Catal.* 7 (2), 1197–1206. doi:10.1021/acscatal.6b02963

Chen, S., Zhang, H., Fu, X., and Hu, Y. (2013). Preparation, characterization, and photocatalytic performance of Ce_2S_3 for nitrobenzene reduction. *Appl. Surf. Sci.* 275, 335–341. doi:10.1016/j.apsusc.2012.12.040

Cheng, H., Long, X., Bian, F., Yang, C., Liu, X., and Jiang, H. (2020). Efficient photocatalytic one-pot hydrogenation and N-alkylation of nitrobenzenes/benzonitriles

with alcohols over Pd/MOFs: Effect of the crystal morphology & "quasi-MOF" structure. *J. Catal.* 389, 121–131. doi:10.1016/j.jcat.2020.05.033

Cui, Z., Zhang, D., Hu, J., and Fang, C. (2021). CdS/CeO_2 heterostructures as visible-light photocatalysts for the reduction of nitro to amine organics. *J. Alloys Compd.* 885, 160961. doi:10.1016/j.jallcom.2021.160961

Daghrir, R., Drogui, P., and Robert, D. (2013). Modified TiO_2 for environmental photocatalytic applications: A review. *Industrial Eng. Chem. Res.* 52 (10), 3581–3599. doi:10.1021/ie303468t

Dhara, A. K., Maity, S., and Dhar, B. B. (2021). Visible-light-mediated synthesis of substituted phenazine and phenoxazinone using Eosin Y as a photoredox catalyst. *Org. Lett.* 23 (9), 3269–3273. doi:10.1021/acs.orglett.1c00725

Dutta, K., Datta, A., and Majumder, S. (2022). Design of plasmonic solar photocatalyst: Judicially coupled hot carrier induced surface plasmon of Ag with graphene. *Opt. Mater.* 123, 111887. doi:10.1016/j.optmat.2021.111887

Eskandari, P., Kazemi, F., and Zand, Z. (2014). Photocatalytic reduction of aromatic nitro compounds using CdS nanostructure under blue LED irradiation. *J. Photochem. Photobiol. A Chem.* 274, 7–12. doi:10.1016/j.jphotochem.2013.09.011

Franchi, D., and Amara, Z. (2020). Applications of sensitized semiconductors as heterogeneous visible-light photocatalysts in organic synthesis. *ACS Sustain. Chem. Eng.* 8 (41), 15405–15429. doi:10.1021/acssuschemeng.0c05179

Fujishima, A., Rao, T. N., and Tryk, D. A. (2000). Titanium dioxide photocatalysis. *J. Photochem. Photobiol. C* 1 (1), 1–21. doi:10.1016/s1389-5567(00)00002-2

Fukui, M., Koshida, W., Tanaka, A., Hashimoto, K., and Kominami, H. (2019). Photocatalytic hydrogenation of nitrobenzenes to anilines over noble metal-free TiO_2 utilizing methylamine as a hydrogen donor. *Appl. Catal. B Environ.* 268, 118446. doi:10.1016/j.apcatb.2019.118446

Gao, W. Z., Xu, Y., Chen, Y., and Fu, W. F. (2015). Highly efficient and selective photocatalytic reduction of nitroarenes using the Ni_2P/CdS catalyst under visible-light irradiation. *Chem. Commun.* 51, 13217–13220. doi:10.1039/c5cc04030b

Gao, Y., Yang, S., Huo, Y., and Hu, X. (2020). Recent progress on reductive coupling of nitroarenes by using organosilanes as convenient reductants. *Adv. Synthesis Catal.* 362 (19), 3971–3986. doi:10.1002/adsc.202000370

Gellé, A., and Moores, A. (2019). Plasmonic nanoparticles: Photocatalysts with a bright future. *Curr. Opin. Green Sustain. Chem.* 15, 60–66. doi:10.1016/j.cogsc.2018.10.002

Ghosh, S., Avellini, T., Petrelli, A., Kriegel, I., Gaspari, R., Almeida, G., et al. (2016). Colloidal $CuFeS_2$ nanocrystals: Intermediate Fe d-band leads to high photothermal conversion efficiency. *Chem. Mater.* 28 (13), 4848–4858. doi:10.1021/acs.chemmater.6b02192

Guo, X., Hao, C., Jin, G., Zhu, H-Y., and Guo, X-Y. (2014). Copper nanoparticles on graphene support: An efficient photocatalyst for coupling of nitroaromatics in visible light. *Angew. Chem. Int. Ed.* 126 (7), 1973–1977. doi:10.1002/anie.201309482

Han, X., He, X., Sun, L., Xiao, H., Chen, J., Xu, J., et al. (2018). Increasing effective photogenerated carriers by *in-situ* anchoring Cu_2O nanoparticles on nitrogen-doped porous carbon yolk-shell cuboctahedral framework. *ACS Catal.* 8 (4), 3348–3356. doi:10.1021/acscatal.7b04219

Huang, X., Zhang, K., Peng, B., Wang, G., and Wang, F. (2021). Ceria-based materials for thermocatalytic and photocatalytic organic synthesis. *ACS Catal.* 11 (15), 9618–9678. doi:10.1021/acscatal.1c02443

Ismael, M. (2020). A review on graphitic carbon nitride (g-C_3N_4) based nanocomposites: Synthesis, categories, and their application in photocatalysis. *J. Alloys Compd.* 846, 156446. doi:10.1016/j.jallcom.2020.156446

Jia, L., Yu, T., and Ye, J. (2022). Mixed metal sulfides for the application of photocatalytic energy conversion. *Energy & Fuels* 36 (19), 11308–11322. doi:10.1021/acs.energyfuels.2c01137

Jiang, C., Shang, Z., and Liang, X. (2015). Chemoselective transfer hydrogenation of nitroarenes catalyzed by highly dispersed, Supported Nickel Nanoparticles. *ACS Catal.* 5 (8), 4814–4818. doi:10.1021/acscatal.5b00969

Jiang, Y., Li, Q., Li, X., Wang, X., Dong, S., Li, J., et al. (2021). Three-dimensional network Pd-Ni/gamma-Al_2O_3 catalysts for highly active catalytic hydrogenation of nitrobenzene to aniline under mild conditions. *ACS Omega* 6 (14), 9780–9790. doi:10.1021/acsomega.1c00441

Jingrun, R., Shi, Z., Qiao, J., Jaroniec, M., and Qiao, S. Z. (2014). Earth-abundant cocatalysts for semiconductor-based photocatalytic water splitting. *Chem. Soc. Rev.* 43, 7787–7812. doi:10.1039/c3cs60425j

Junhua, W., Zhenle, Y., Renfeng, N., Hou, Z., and Zheng, X. (2010). Hydrogenation of nitrobenzene to aniline over silica gel supported nickel catalysts. *Industrial Eng. Chem. Res.* 49 (10), 4664–4669. doi:10.1021/ie1002069

Kamegawa, T., Seto, H., Matsuura, S., and Yamashita, H. (2012). Preparation of hydroxynaphthalene-modified TiO_2 via formation of surface complexes and their applications in the photocatalytic reduction of nitrobenzene under visible-light irradiation. *ACS Appl. Mater. Interfaces* 4 (12), 6635–6639. doi:10.1021/am3017762

Kandiel, T. A., Ivanova, I., and Bahnemann, D. W. (2014). Long-term investigation of the photocatalytic hydrogen production on platinized TiO_2: An isotopic study. *Energy & Environ. Sci.* 7 (4), 1420–1425. doi:10.1039/c3ee41511b

Kavitha, R., and Kumar, S. G. (2019). A review on plasmonic Au-ZnO heterojunction photocatalysts: Preparation, modifications and related charge carrier dynamics. *Mater. Sci. Semicond. Process.* 93, 59–91. doi:10.1016/j.mssp.2018.12.026

Kou, J., Lu, C., Wang, J., Chen, Y., Xu, Z., and Varma, R. S. (2017). Selectivity enhancement in heterogeneous photocatalytic transformations. *Chem. Rev.* 117 (3), 1445–1514. doi:10.1021/acs.chemrev.6b00396

Kouser, S., Hezam, A., and Khanum, S. A. (2023). Rational design and engineering of efficient metal organic framework for visible light-driven photocatalytic carbon dioxide reduction. *Inorganica Chim. Acta* 546 (1), 121287. doi:10.1016/j.ica.2022.121287

Kudo, A., and Miseki, Y. (2008). Heterogeneous photocatalyst materials for water splitting. *Chem. Soc. Rev.* 38 (1), 253–278. doi:10.1039/b800489g

Kw, A., Song, S. A., Min, C. A., Jl, A., Kai, Z. C., Jian, P. B., et al. (2020). Pd-TiO_2 Schottky heterojunction catalyst boost the electrocatalytic hydrodechlorination reaction. *Chem. Eng. J.* 381, 122673. doi:10.1016/j.cej.2019.122673

Lang, X., Chen, X., and Zhao, J. (2014). Heterogeneous visible light photocatalysis for selective organic transformations. *Chem. Soc. Rev.* 43, 473–486. doi:10.1039/c3cs60188a

Li, C., Li, J., Huang, Y., Liu, J., Ma, M., Liu, K., et al. (2022). Recent development in electronic structure tuning of graphitic carbon nitride for highly efficient photocatalysis. *J. Semicond.* 43 (2), 021701–021734. doi:10.1088/1674-4926/43/2/021701

Li, F., Wen, C., Wang, A., and Zheng, Y. (2015). Photocatalytic hydrogenation of nitrobenzene to aniline over tungsten oxide-silver nanowires. *Mater. Lett.* 142, 201–203. doi:10.1016/j.matlet.2014.12.021

Li, J. Y., Li, Y. H., Qi, M. Y., Lin, Q., and Xu, Y. J. (2020). Selective organic transformations over cadmium sulfide-based photocatalysts. *ACS Catal.* 10 (11), 6262–6280. doi:10.1021/acscatal.0c01567

Li, X., Dong, Q., Tian, Q., Sial, A., Wang, H., Wen, H., et al. (2022). Recent advance in metal- and covalent-organic framework-based photocatalysis for hydrogen evolution. *Mater. Today Chem.* 26, 101037. doi:10.1016/j.mtchem.2022.101037

Liao, G., Li, C., Li, X., and Fang, B. (2021). Emerging polymeric carbon nitride Z-scheme systems for photocatalysis. *Cell Rep. Phys. Sci.* 2 (3), 100355. doi:10.1016/j.xcrp.2021.100355

Lin, Z., Ji, L., Wu, Y., Hu, L., Yan, T., and Sun, Z. (2019). Laser-induced interfacial state changes enable tuning of the Schottky-barrier height in SiC. *Appl. Surf. Sci.* 469, 68–75. doi:10.1016/j.apsusc.2018.11.015

Liu, Q., Li, Z., Liu, Q., Cheng, C., Song, M., and Huang, A. (2020). Photocatalysis under shell: Co@BN core-shell composites for efficient EY-sensitized photocatalytic hydrogen evolution. *Appl. Surf. Sci.* 514, 146096. doi:10.1016/j.apsusc.2020.146096

Lu, C., Yin, Z., Sun, C., Chen, C., and Wang, F. (2021). Photocatalytic reduction of nitroaromatics into anilines using CeO_2-TiO_2 nanocomposite. *Mol. Catal.* 513, 111775. doi:10.1016/j.mcat.2021.111775

Ma, B., Wang, Y., Tong, X., Guo, X., Zheng, Z., and Guo, X. (2017). Graphene-supported CoS_2 particles: An efficient photocatalyst for selective hydrogenation of nitroaromatics in visible light. *Catal. Sci. Technol.* 7 (13), 2805–2812. doi:10.1039/c7cy00356k

Maji, T., Karmakar, A., and Reiser, O. (2011). Visible-light photoredox catalysis: Dehalogenation of vicinal dibromo-α-halo-and α,α-dibromocarbonyl compounds. *J. Org. Chem.* 76 (2), 736–739. doi:10.1021/jo102239x

Murali, G., Modigunta, J. K. R., Park, Y. H., Lee, J. H., Rawal, J., Lee, S. Y., et al. (2022). A review on Mxene synthesis, stability, and photocatalytic applications. *ACS Nano* 16 (9), 13370–13429. doi:10.1021/acsnano.2c04750

Ojha, N., Metya, A. K., and Kumar, S. (2021). Influence of plasmonic metals (Ag, Cu) on overall CO_2 photoreduction activity of β-Ga_2O_3. *Appl. Surf. Sci.* 580, 152315. doi:10.1016/j.apsusc.2021.152315

Oliveira, A. G., Nascimento, J. P., Gorgulho, H. F., Martelli, P. B., Furtado, C. A., and Figueiredo, J. L. (2016). Electrochemical synthesis of TiO_2/graphene oxide composite films for photocatalytic applications. *J. Alloys Compd.* 654, 514–522. doi:10.1016/j.jallcom.2015.09.110

Patel, S. B., Tripathi, A., and Vyas, A. P. (2021). Recent development in the structural modification of graphitic carbon nitride for sustainable photocatalysis: Advances, challenges and opportunities. *Environ. Nanotechnol. Monit. Manag.* 16, 100589. doi:10.1016/j.enmm.2021.100589

Pei, L., Tan, H., Liu, M., Wang, R., Gu, X., Ke, X., et al. (2021). Hydroxyl-group-modified polymeric carbon nitride with the highly selective hydrogenation of nitrobenzene to N-phenylhydroxylamine under visible light. *Green Chem.* 23 (10), 3612–3622. doi:10.1039/d1gc00325a

Poulose, A. C., Zoppellaro, G., Konidakis, I., Serpetzoglou, E., and Zboil, R. (2022). Fast and selective reduction of nitroarenes under visible light with an earth-abundant plasmonic photocatalyst. *Nat. Nanotechnol.* 17 (5), 1–8.

Prasad, C., Liu, Q., Tang, H., Yuvaraja, G., Long, J., Rammohan, A., et al. (2020). An overview of graphene oxide supported semiconductors based photocatalysts: Properties, synthesis and photocatalytic applications. *J. Mol. Liq.* 297, 111826. doi:10.1016/j.molliq.2019.111826

Qiu, B., Deng, Y., Li, Q., Shen, B., and Zhang, J. (2016). Rational design of a unique ternary structure for highly photocatalytic nitrobenzene reduction. *J. Phys. Chem. C* 120 (22), 12125–12131. doi:10.1021/acs.jpcc.6b03800

Qiu, B., Xing, M., and Zhang, J. (2014). Mesoporous TiO_2 nanocrystals grown *in situ* on graphene aerogels for high photocatalysis and lithium-ion batteries. *J. Am. Chem. Soc.* 136 (16), 5852–5855. doi:10.1021/ja500873u

Ramezanalizadeh, H., and Rafiee, E. (2020). Design, fabrication, electro- and photoelectrochemical investigations of novel $CoTiO_3/CuBi_2O_4$ heterojunction semiconductor: An efficient photocatalyst for the degradation of DR16 dye. *Mater. Sci. Semicond. Process.* 113, 105055. doi:10.1016/j.mssp.2020.105055

Ranjith, K. S., Saravanan, P., Vinod, V., Filip, J., Černík, M., and Kumar, R. R. (2016). Ce_2S_3 decorated ZnO-ZnS core-shell nanorod arrays: Efficient solar-driven photocatalytic properties. *Catal. Today* 278, 271–279. doi:10.1016/j.cattod.2016.05.011

Rauf, H. T., Yasmin, N., Ali, G., Ashiq, M. N., Safdar, M., and Mirza, M. (2022). New insight in photocatalytic degradation of textile dyes over CeO_2/Ce_2S_3 composite. *Phys. B Condens. Matter* 632, 413760. doi:10.1016/j.physb.2022.413760

Roy, S. (2020). Photocatalytic materials for reduction of nitroarenes and nitrates. *J. Phys. Chem. C* 52 (124), 28345–28358. doi:10.1021/acs.jpcc.0c07363

Shen, Z., Hu, Y., Li, B., Zou, Y., Muhler, M., Wilma Busser, G., et al. (2021). State-of-the-art progress in the selective photo-oxidation of alcohols. *J. Energy Chem.* 62, 338–350. doi:10.1016/j.jechem.2021.03.033

Shi, Y., Ma, J., Chen, Y., Qian, Y., Xu, B., Chu, W., et al. (2022). Recent progress of silver-containing photocatalysts for water disinfection under visible light irradiation: A review. *Sci. Total Environ.* 804, 150024. doi:10.1016/j.scitotenv.2021.150024

Shiraishi, Y., Togawa, Y., Tsukamoto, D., Tanaka, S., and Hirai, T. (2012). Highly efficient and selective hydrogenation of nitroaromatics on photoactivated rutile titanium dioxide. *ACS Catal.* 2 (12), 2475–2481. doi:10.1021/cs300500p

Silva, A., Rodrigues, T. S., Wang, J., and Camargo, P. (2022). Plasmonic catalysis with designer nanoparticles. *Chem. Commun.* 58 (13), 2055–2074. doi:10.1039/d1cc03779j

Sugathan, A., Bhattacharyya, B., Kishore, V. V. R., Kumar, A., Pandey, A., Sarma, D. D., et al. (2018). Why does $CuFeS_2$ resemble gold? *J. Phys. Chem. Lett.* 9 (4), 696–701. doi:10.1021/acs.jpclett.7b03190

Tamaki, Y., Furube, A., Murai, M., Hara, K., Katoh, R., and Tachiya, M. (2007). Dynamics of efficient electron-hole separation in TiO_2 nanoparticles revealed by femtosecond transient absorption spectroscopy under the weak-excitation condition. *Phys. Chem. Chem. Phys.* 9 (12), 1453–1460. doi:10.1039/b617552j

Tang, J., Gao, B., Pan, J., Chen, L., Yin, S. F., Shen, S., et al. (2019). CdS nanorods anchored with CoS_2 nanoparticles for enhanced photocatalytic hydrogen production. *Appl. Catal. A General* 588, 117281. doi:10.1016/j.apcata.2019.117281

Tsutsumi, K., Uchikawa, F., Sakai, K., and Tabata, K. (2016). Photoinduced reduction of nitroarenes using a transition-metal-loaded silicon semiconductor under visible light irradiation. *ACS Catal.* 6 (7), 4394–4398. doi:10.1021/acscatal.6b00886

Wang, C., Li, A., Li, C., Zhang, S., Li, H., Zhou, X., et al. (2019). Ultrahigh photocatalytic rate at a single-metal-atom-oxide. *Adv. Mater.* 31 (52), 1903491. doi:10.1002/adma.201903491

Wang, H., Zhang, X., and Xie, Y. (2018). Photoresponsive polymeric carbon nitride-based materials: Design and application. *Mater. Today* 23, 72–86. doi:10.1016/j.mattod.2018.05.001

Wang, J. H., Zhang, Y., Li, M., Yan, S., Li, D., and Zhang, X. M. (2017). Solvent-assisted metal metathesis: A highly efficient and versatile route towards synthetically demanding chromium metal-organic frameworks. *Angew. Chem. Int. Ed.* 129 (23), 6578–6582. doi:10.1002/ange.201701217

Wang, W., Xue, K., Pan, P., and Duan, J. (2019). Preparation of bifunctional core-shell structured Cu/TS-1@MCM-41 molecular sieves for synthesis of aniline by benzene in one step amination. *Microporous Mesoporous Mater.* 277, 163–170. doi:10.1016/j.micromeso.2018.10.038

Wang, W. K., Chen, J., Li, W. W., Pei, D. N., Zhang, X., and Yu, H. Q. (2015). Synthesis of Pt-loaded self-interspersed anatase TiO_2 with a large fraction of (001) facets for efficient photocatalytic nitrobenzene degradation. *ACS Appl. Mater. Interfaces* 7 (36), 20349–20359. doi:10.1021/acsami.5b06161

Wang, Y., Liu, B., Wang, Y., Yuan, H., and Peng, X. (2021). Plasmonic semiconductor: A tunable non-metal photocatalyst. *Int. J. Hydrogen Energy* 46 (58), 29858–29888. doi:10.1016/j.ijhydene.2021.06.142

Wang, Y., Mo, Z., Zhang, P., Zhang, C., Han, L., Guo, R., et al. (2016). Synthesis of flower-like TiO_2 microsphere/graphene composite for removal of organic dye from water. *Mater. Des.* 99, 378–388. doi:10.1016/j.matdes.2016.03.066

Wang, Z., Zhang, Y., Neyts, E. C., Cao, X., Zhang, X., Jang, B. W. L., et al. (2018). Catalyst preparation with plasmas: How does it work? *ACS Catal.* 8 (3), 2093–2110. doi:10.1021/acscatal.7b03723

Wei, H., Liu, X., Wang, A., Zhang, L., Qiao, B., Yang, X., et al. (2014). FeO_x-supported platinum single-atom and pseudo-single-atom catalysts for chemoselective hydrogenation of functionalized nitroarenes. *Nat. Commun.* 5, 5634. doi:10.1038/ncomms6634

Wudil, Y. S., Ahmad, U. F., Gondal, M. A., Al-Osta, M. A., Almohammedi, A., Sa'id, R., et al. (2023). Tuning of graphitic carbon nitride (g-C_3N_4) for photocatalysis: A critical review. *Arabian J. Chem.* 16 (3), 104542. doi:10.1016/j.arabjc.2023.104542

Xiao, F. X., Miao, J., and Liu, B. (2014). Layer-by-layer self-assembly of CdS quantum dots/graphene nanosheets hybrid films for photoelectrochemical and photocatalytic applications. *J. Am. Chem. Soc.* 136 (4), 1559–1569. doi:10.1021/ja411651e

Xiao, G., Li, P., Zhao, Y., Xu, S., and Su, H. (2018). Visible-light-driven chemoselective hydrogenation of nitroarenes to anilines in water through graphitic carbon nitride metal-free photocatalysis. *Chemistry-an Asian J.* 13, 1950–1955. doi:10.1002/asia.201800515

Xie, G., Song, F., Zhu, Y., Wang, X., Wang, J., Wu, Z., et al. (2022). A study on the role of plasmonic $Ti_3C_2T_x$ MXene in enhancing photoredox catalysis. *Nanoscale* 14 (48), 18010–18021. doi:10.1039/d2nr05983e

Xin, Y., Yu, K., Zhang, L., Yang, Y., Yuan, H., Li, H., et al. (2021). Copper-based plasmonic catalysis: Recent advances and future perspectives. *Adv. Mater.* 33 (32), 2008145. doi:10.1002/adma.202008145

Xu, D., Zhang, S. N., Chen, J. S., and Li, X. H. (2023). Design of the synergistic rectifying interfaces in Mott–Schottky catalysts. *Chem. Rev.* 123 (1), 1–30. doi:10.1021/acs.chemrev.2c00426

Xu, F., Meng, K., Cao, S., Jiang, C., Chen, T., Xu, J., et al. (2021). Step-by-step mechanism insights into the TiO_2/Ce_2S_3 S-scheme photocatalyst for enhanced aniline production with water as a proton source. *ACS Catal.* 12 (1), 164–172. doi:10.1021/acscatal.1c04903

Xu, Q., Wageh, S., Al-Ghamdi, A. A., and Li, X. (2022). Design principle of S-scheme heterojunction photocatalyst. *J. Mater. Sci. Technol.* 124, 171–173. doi:10.1016/j.jmst.2022.02.016

Xu, S., Tang, J., Zhou, Q., Du, J., and Li, H. (2019). Interfacing anatase with carbon layers for photocatalytic nitroarene hydrogenation. *ACS Sustain. Chem. Eng.* 7 (19), 16190–16199. doi:10.1021/acssuschemeng.9b03149

Xu, Y., and Schoonen, M. (2000). The absolute energy positions of conduction and valence bands of selected semiconducting minerals. *Am. Mineralogist* 85 (3-4), 543–556. doi:10.2138/am-2000-0416

Xuan, J., and Xiao, P. D. W-J. (2012). Visible-light photoredox catalysis. *Angew. Chem. Int. Ed.* 51 (28), 6828–6838. doi:10.1002/anie.201200223

Yang, H. (2021). A short review on heterojunction photocatalysts: Carrier transfer behavior and photocatalytic mechanisms. *Mater. Res. Bull.* 142, 111406. doi:10.1016/j.materresbull.2021.111406

Yang, X. J., Chen, B., Zheng, L. Q., Wu, L. Z., and Tung, C. H. (2014). Highly efficient and selective photocatalytic hydrogenation of functionalized nitrobenzenes. *Green Chem.* 16 (3), 1082–1086. doi:10.1039/c3gc42042f

Yang, Y., Li, H., Jing, X., Wu, Y., Shi, Y., and Duan, C. (2022). Dye-loaded metal-organic helical capsules applied to the combination of photocatalytic H_2S splitting and nitroaromatic hydrogenation. *Chem. Commun.* 58, 807–810. doi:10.1039/d1cc06166f

Ye, X., Dai, X., Meng, S., Fu, X., and Chen, S. (2017). A novel CdS/g-C_3N_4 composite photocatalyst: Preparation, characterization and photocatalytic performance with different reaction solvents under visible light irradiation. *Chin. J. Chem.* 35 (2), 217–225. doi:10.1002/cjoc.201600251

Yu, C., Peng, L., Zhu, Y., Xie, G., Wu, Z., and Xie, X. (2021). Electrostatically confined $Bi/Ti_3C_2T_x$ on a sponge as an easily recyclable and durable catalyst for the reductive transformation of nitroarenes. *R. Soc. Chem.* 35, 19847–19853.

Yu, W., Guo, X., Song, C., and Zhao, Z. (2019). Visible-light-initiated one-pot clean synthesis of nitrone from nitrobenzene and benzyl alcohol over CdS photocatalyst. *J. Catal.* 370, 97–106. doi:10.1016/j.jcat.2018.12.011

Yun, G., Hyla, B., Yhya, B., Jie, H., Jiang, D., and Bing, X. (2020). Microemulsion extraction: An efficient way for simultaneous detoxification and resource recovery of hazardous wastewater containing V(V) and Cr(VI). *J. Hazard. Mater.* 386, 121948. doi:10.1016/j.jhazmat.2019.121948

Žerjav, G., Roškarič, M., Zavašnik, J., Kovač, J., and Pintar, A. (2021). Effect of Au loading on Schottky barrier height in TiO_2 +Au plasmonic photocatalysts. *Appl. Surf. Sci.* 579, 152196.

Zhang, C., and Zhu, Y. (2005). Synthesis of square Bi_2WO_6 nanoplates as high-activity visible-light-driven photocatalysts. *Chem. Mater.* 17 (13), 3537–3545. doi:10.1021/cm0501517

Zhang, N., Zhang, Y., Pan, X., Fu, X., and Xu, Y. J. (2011). Assembly of CdS nanoparticles on the two-dimensional graphene scaffold as visible-light-driven photocatalyst for selective organic transformation under ambient conditions. *J. Phys. Chem. C* 115 (47), 23501–23511. doi:10.1021/jp208661n

Zhang, S., Ou, X., Xiang, Q., Carabineiro, S., Fan, J., and Lv, K. (2022). Research progress in metal sulfides for photocatalysis: From activity to stability. *Chemosphere* 303, 135085. doi:10.1016/j.chemosphere.2022.135085

Zhang, T., Jin, Y., Shi, Y., Li, M., Li, J., and Duan, C. (2019). Modulating photoelectronic performance of metal-organic frameworks for premium photocatalysis. *Coord. Chem. Rev.* 380, 201–229. doi:10.1016/j.ccr.2018.10.001

Zhang, Y., Yuan, C., Wang, Q., Hoffmann, M. R., Cong, Y., Nie, J., et al. (2019). Photoelectrochemical activity of CdS/Ag/TiO_2 nanorod composites: Degradation of nitrobenzene coupled with the concomitant production of molecular hydrogen. *Electrochimica Acta* 328, 135124. doi:10.1016/j.electacta.2019.135124

Zhao, X., Yue, S., Zhang, J., Zhao, C., Wu, Y., Shan, D., et al. (2022). Classification and catalytic mechanisms of heterojunction photocatalysts and the application of titanium dioxide (TiO_2)-based heterojunctions in environmental remediation. *J. Environ. Chem. Eng.* 10 (3), 108077. doi:10.1016/j.jece.2022.108077

Zhao, Z., Wu, H., and Li, C. (2021). Engineering iron phosphide-on-plasmonic Ag/Au-nanoshells as an efficient cathode catalyst in water splitting for hydrogen production. *Energy* 218, 119520. doi:10.1016/j.energy.2020.119520

Zheng, Z., Tachikawa, T., and Majima, T. (2014). Single-particle study of Pt-modified Au nanorods for plasmon-enhanced hydrogen generation in visible to near-infrared region. *J. Am. Chem. Soc.* 136 (19), 6870–6873. doi:10.1021/ja502704n

Zhou, B-X., Huang, W-Q., Yang, K., Ding, S-S., Xie, Z., Pan, A., et al. (2018). Theory-driven heterojunction photocatalyst design with continuously adjustable band gap materials. *J. Phys. Chem. C* 122 (49), 28065–28074. doi:10.1021/acs.jpcc.8b08060

Zhou, D., Li, D., Yuan, S., and Chen, Z. (2022). Recent advances in biomass-based photocatalytic H_2 production and efficient photocatalysts: A review. *Energy & Fuels* 36 (18), 10721–10731. doi:10.1021/acs.energyfuels.2c01904

Zhu, P. H., Ke, X., Yang, P. D. X., Sarina, S., and Liu, H. (2010). Reduction of nitroaromatic compounds on supported gold nanoparticles by visible and ultraviolet light. *Angew. Chem. Int. Ed.* 49 (50), 9851–9855. doi:10.1002/ange.201003908